

Inference of postseismic deformation mechanisms of the 1923 Kanto earthquake

Fred F. Pollitz¹, Marleen C.J. Nyst¹, Takuya Nishimura², and Wayne Thatcher¹

¹*U.S. Geological Survey
345 Middlefield Rd., MS 977
Menlo Park, CA 94025
U.S.A.*

²*Geographical Survey Institute
Geography and Crustal Dynamics Research Center
Tsukuba, Japan*

Revised Version
J. Geophys. Res.
October, 2005

Abstract

Coseismic slip associated with the M7.9 1923 Kanto earthquake is fairly well understood, involving slip of up to 8 meters along the Philippine Sea - Honshu interplate boundary under Sagami Bay and its onland extension. Postseismic deformation after the 1923 earthquake, however, is relatively poorly understood. We re-visit the available deformation data in order to constrain possible mechanisms of postseismic deformation and to examine the consequences for associated stress changes in the surrounding crust. Data from two leveling lines, one tide gage station, and a small aperture strain array (Mitaka Rhombus) over the first 7 to 8 years postseismic period are of much greater amplitude than the corresponding expected interseismic deformation during the same period, making these data suitable for isolating the signal from postseismic deformation. We consider both viscoelastic models of asthenosphere relaxation and afterslip models. A distributed coseismic slip model presented in Pollitz et al. (2005), combined with prescribed parameters of a viscoelastic Earth model, yields predicted postseismic deformation that agrees with observed deformation on mainland Honshu from Tokyo to the Izu peninsula. Elsewhere (southern Miura peninsula; Boso peninsula), the considered viscoelastic models fail to predict observed deformation, and a model of ~1 meter shallow afterslip in the offshore region south of the Boso peninsula, with equivalent moment magnitude $M_w=7.0$, adequately accounts for the observed deformation. Using the distributed coseismic slip model, layered viscoelastic structure, and a model of interseismic strain accumulation, we evaluate the post-1923 stress evolution, including both the coseismic and accumulated postseismic stress changes and those stresses contributed by interseismic loading. We find that if account is made for the varying tectonic regime in the region, the occurrence of both immediate (first month) post-1923 crustal aftershocks as well as recent regional crustal seismicity is consistent with the predicted stress pattern. This suggests that the influence of the 1923 earthquake on regional seismicity is fairly predictable and has persisted for at least seven decades following the earthquake.

1 Introduction

The region of the M7.9 1 September, 1923 Kanto earthquake lies at the complex junction between three tectonic plates (Figure 1): the Philippine Sea plate (PHS), the

Pacific plate (PAC), and northeast Honshu. The Itoigawa-Shizuoka Tectonic Line (ISTL) is considered to be a major fault dividing central Honshu from northeast Honshu. Different authors consider that central Japan belongs to the Amurian or Eurasian plates (e.g., Nakamura, 1983; Heki et al., 1999), and similarly that northeast Honshu belongs to the North American plate or Okhotsk plate (e.g., Seno et al., 1996; Heki et al., 1999). We shall refer here to northeast Honshu as simply the Honshu plate. The convergence rates between the PHS and Honshu plates is 3 to 4 cm/yr (Yoshioka et al., 1994; Mazzotti et al., 2001) and between the PAC and the Honshu plates is about 8 cm/yr (DeMets et al., 1990; Seno et al., 1996), making this region one of intense strain accumulation. The 1923 earthquake involved about 6 to 8 meters of slip along the PHS-Honshu interplate boundary, which is a subduction zone dipping 20° to 40° to the NE. The effective backslip accumulation rate on the PHS-Honshu interface is between 3 and 4 cm/yr (Yoshioka, 1992; Mazzotti et al., 2001; Sagiya, 2004; Nishimura and Sagiya, 2005), which is comparable with the ~ 4 cm/yr relative plate motion between the PHS and Eurasian plates. Thus the 1923 earthquake relieved about 200 to 300 years of strain accumulation, and it is a defining event for the recent crustal stress evolution.

In Nyst et al. (2005), the basic geometry of faulting involved in the Kanto earthquake was defined, and an optimal slip distribution derived from a large coseismic triangulation and leveling dataset. The coseismic slip involves a combination of dip slip and strike slip on two resolvable $\sim 20 - 30^{\circ}$ dipping planes (Figures 2a and 2b), with approximately a 3:1 ratio between thrust and right-lateral strike-slip motion. This is consistent with the sense of strain accumulation involving NNW motion of PHS relative to Honshu (Mazzotti et al., 2000; Sagiya, 2004). The two fault planes are very similar to those defined by Model III of Matsu'ura et al. (1980). A more detailed slip inversion (Pollitz et al., 2005) allowing for distributed slip on two larger planes, inclusive of these two planes, reveals the possibility of additional coseismic slip SE of the larger fault as well as a slight change in rake from NW to SE along the larger fault.

In order to understand the impact of this earthquake on the regional stress evolution, it is important to study not only the coseismic deformation but also the postseismic deformation. Study of the mechanisms of postseismic deformation of the Kanto earthquake is challenging for several reasons. The mechanisms governing postseismic

deformation are comparatively poorly understood relative to those involved in coseismic deformation. The amount of information in the postseismic period that can shed light on the mechanisms of postseismic deformation is relatively small compared with that available for the coseismic deformation (Nyst et al., 2005). Very different postseismic mechanisms, such as afterslip and viscoelastic relaxation, often yield predicted surface deformation that are nearly indistinguishable from one another. Much of the faulting that was associated with the Kanto earthquake occurred well out to sea, and continued slip in these regions at reduced amplitudes may be difficult to detect and resolve with land measurements.

These issues may help explain why previous studies have reached somewhat different conclusions concerning the mechanisms of postseismic deformation after the Kanto earthquake. Scholz and Kato (1978) investigated postseismic deformation mechanisms by employing the coseismic fault model of Ando (1974) and considering leveling data along the Boso peninsula and along the Tokyo-Atami route. By assuming that these observations could be adequately modeled as a two-dimensional problem, they derived a model of postseismic afterslip along the coseismic rupture plane in the sense opposite to the coseismic slip, i.e., normal faulting. Thatcher and Rundle (1979) employed the coseismic fault model of Ando (1971) and used the Boso Peninsula and Tokyo-Atami leveling data plus tide gage data to derive a model of viscoelastic relaxation for the first ~8 years postseismic period (1923 to 1931). It involves relaxation of an elastic plate of thickness 60 km underlain by a halfspace asthenosphere of viscosity 6×10^{19} Pa s. Further consideration of strain data from the Mitaka Rhombus near Tokyo led them to identify afterslip in the deeper extension of the NW part of the coseismic rupture plane during the early postseismic period (September, 1923 - September, 1924). Matsu'ura and Iwasaki (1983) also investigated a viscoelastic relaxation mechanism for the postseismic deformation. They adopted the Kanamori (1971) coseismic fault model and considered the Kanto area leveling observed from 1931 to 1950, excluding the Boso peninsula. They derived a model of relaxation of a 60 km thick elastic layer underlain by a halfspace asthenosphere of viscosity 10^{19} Pa s.

The above models have addressed essentially all of the relevant data that may constrain postseismic deformation mechanisms, but they come to different conclusions. In large part this stems from the different data used by different investigators, and to a smaller extent results from the different coseismic fault models that were employed. In

the present study we re-evaluate the postseismic mechanisms of the 1923 earthquake by considering a combination of postseismic leveling data, tide gage data, and strain data (Mitaka Rhombus). In addition, to drive possible viscoelastic relaxation of the asthenosphere we use the distributed coseismic fault model derived in Pollitz et al. (2005). We find that viscoelastic relaxation effects are sufficient to explain the Tokyo-Atami leveling data, but not sufficient to explain either the Boso leveling data or tide gage data. To explain them we advocate a model of shallow afterslip in the SE portion of the coseismic rupture plane, located offshore Boso peninsula.

2 Postseismic Data

Figure 3 shows the locations of the leveling lines, tide gage station, and a 100 m-aperture array (Mitaka Rhombus) used in this study. Figure 3 shows the cumulative displacement measured across the two leveling lines. The leveling data have been extracted from the database of the Geographical Survey Institute and are described in Military Land Survey (1930). They cover the periods 1923 - 1931 and 1923 - 1930 along the Boso Peninsula and Tokyo - Atami routes, respectively. The cumulative displacement profiles are shown in Figure 3 and are similar to those derived from the same data set by Scholz and Kato (1978) and Thatcher and Rundle (1979). Errors associated with a single section height measurement of 1 km length are of order 0.7 mm. Since errors accumulate along a line upon summation of the section height difference, the cumulative displacement is associated with errors that increase with distance along the line. Factoring in the differencing of the common measurements made at two different times, the cumulative displacement errors reach a maximum of about 10 mm. Each leveling route contains signals of order several cm during the first ~8 years postseismic time interval. This is much larger than the interseismic uplift rate as constrained by later leveling profiles (e.g., Dambara and Hirobe, 1964) and 1996-1999 GPS data (Aoki and Scholz, 2003).

Figure 4 shows a time series of monthly sea level height measurements made at Aburatsubo tide station since 1896. The postseismic interval of interest, 1924 to 1931, contains signals due to both tectonic postseismic activity as well as background sea level changes. We assume that the latter can be adequately estimated by fitting a line through the measurements made from 1950 to 2000. If the standard error associ-

ated with a single tidal measurement is assigned the value 50 mm, then after propagation of errors the resulting slopes of best-fitting lines using data from the 1923-1931 and 1950-2000 epochs are 8.2 ± 6.2 mm/yr and 2.2 ± 0.4 mm/yr. If the former is corrected by the latter, then the tectonic postseismic signal accumulated during the first 7 year postseismic time interval amounts to 4.2 ± 4.3 cm subsidence. The 1896 to 1923 time interval could also be used to estimate the interseismic sea level rise rate, and fitting the slope for this time period yields 4.4 ± 0.9 mm/yr. If this value were used for the interseismic correction, then we would obtain a postseismic signal of 2.8 ± 4.3 cm subsidence during the first 7 year postseismic time interval. We prefer to make the correction using the rate obtained with the 1950-2000 time interval because the tide time series contains harmonic signals which have not been removed, and it is preferable to use a longer time interval in order to average out these non-tectonic signals. The formal standard deviation of 4.3 cm would appear to render the estimated subsidence insignificantly different from zero. However, much of the scatter in sea-level time series arises from deterministic signals with a periodicity of one year (e.g., Barbosa et al., 2004), and such signal would be averaged out more effectively than a purely random one.

Repeated horizontal measurements were conducted at four sites on the Mitaka Rhombus (location indicated in Figure 2a) from 1916 to 1980. This dataset, which has been discussed in detail by Fujita and Thatcher (1984), yields time-dependent strain components e_{11} , e_{12} , and e_{22} , where 1 and 2 denote the local due East and North directions, respectively (Figure 5). This dataset provides valuable information on the postseismic deformation field as it is the only available source of horizontal postseismic deformation during the first two decades following the 1923 earthquake. (Triangulation data from 1923 to 1951 are inadequate to capture any useful signal in the horizontal postseismic deformation field.) Owing to the geometry of the Mitaka benchmarks, errors are somewhat larger for the e_{22} component compared with the e_{11} and e_{12} components. As noted by Fujita and Thatcher (1984), the largest signal is seen in the e_{22} component which exhibits a rapid north-south contraction during the first year after the 1923 earthquake, followed by a ~ 5 - year period of north-south extension. The e_{11} component exhibits a similar pattern but with opposite sign and smaller magnitude.

3 Mechanisms of postseismic deformation

The vertical deformation recorded by both the leveling measurements and tide station during the first 8 years after the 1923 earthquake contain tectonic signals much larger than the interseismic deformation over the considered time period. Two possible postseismic processes contributing to the observed rapid postseismic deformation rates are afterslip and viscoelastic relaxation of the asthenosphere (Figure 6). In the afterslip model, continued slip on the 1923 fault surface or its extension in the down-dip or updip direction could occur as an addition to the coseismic slip. In the viscoelastic relaxation model, a ductile mantle underlying the Honshu lithosphere is expected to relax the coseismic stress changes imparted by the 1923 earthquake, resulting in continued deformation of the mechanical lithosphere. Both processes may contribute in varying degrees to observed postseismic deformation. Discrimination between the two may shed light on the susceptibility of the plate boundary to accommodate aseismic slip and, if that is the case, whether it occurs at shallow or deep levels.

3.1 Viscoelastic relaxation

In order to gain an understanding of the behavior of the postseismic viscoelastic relaxation fields possibly generated by the 1923 earthquake, we consider two examples with synthetic faults. We choose elastic parameters given by Sato et al. (1998) (Figure 7), and prescribe an elastic layer of thickness H_e underlain by a viscoelastic asthenosphere of viscosity η (Figures 7 and 8). Referring to Figure 8, we prescribe a 100 km-long fault dipping towards the right with dip of either 45° or 23° , with upper and lower edge depths of 5 km and 30 km, respectively, and a rake of 153° , i.e., a 2:1 ratio in strike-slip to dip-slip motion. This example takes an elastic plate thickness of $H_e=50$ km and mantle viscosity of $\eta = 10^{19}$ Pa s. Postseismic deformation is calculated using the method of Pollitz (1997). The resulting postseismic displacement patterns (Figure 8) are asymmetric with respect to the center of the fault because of the strike-slip component, with greatest subsidence at the fault end closest to the strike direction and greatest uplift at the fault end farthest from the strike direction. The amplitude of postseismic subsidence is greater in the 23° dipping case than the 45° dipping case, though the overall amplitudes of several cm are roughly consistent with observed postseismic uplift/subsidence (Figures 4 and 5). The input parameters in

these examples are similar to, but not identical to, those used by Matsu'ura and Iwasaki (1983) in their forward calculation of post-1923 relaxation. However, one can notice the similarity in the pattern of Figure 8 (23° dipping case) with that of Figure 6d of Matsu'ura and Iwasaki (1983).

We calculate a forward model of postseismic relaxation for the first 8 years using the Ando (1971) coseismic rupture model and viscoelastic parameters $H_e=60$ km and $\eta=6\times 10^{19}$ Pa s. This was the fault model employed by Thatcher and Rundle (1979), who calculated the postseismic uplift pattern for the same time period using identical H_e and η . The only difference between the present calculation and that of Thatcher and Rundle is that we employ a layered Earth model, and the shear modulus in the relaxing asthenosphere is 63 GPa in our model (Figure 7) and 60 GPa in the Thatcher and Rundle (1979) model. The result of our forward model is shown in Figure 9, and a comparison of the calculated with observed postseismic vertical displacement along the leveling lines is shown in Figure 10a. The quantity NMRS in the parts of Figure 10 is the normalized root-mean square difference between calculated and observed uplift at the leveling sites along a given route:

$$NRMS = \left\{ \frac{1}{N-n} \sum_{i=1}^N \left[u_z^{(i)} |_{\text{cal}} - u_z^{(i)} |_{\text{obs}} \right]^2 \right\}^{1/2} \quad (1)$$

where N is the number of leveling points ($N=78$ on the Boso profile, $N=48$ on the Tokyo-Atami profile), $n=6$ is the number of parameters needed to describe uniform slip on a fault plane. Qualitatively the shape of the calculated leveling profiles is similar to those calculated in Thatcher and Rundle (1979) but with much reduced amplitude. To understand this discrepancy, it is possible that some aspect of the input parameters used by Thatcher and Rundle differs from those used here. More likely, Thatcher and Rundle (1979) assumed pure dip-slip fault motion. We regard this as the more plausible explanation because the corresponding model prediction of the pure-dip slip case, other factors being equal, is found to be of much larger amplitude and to match the predicted postseismic uplift curve of Thatcher and Rundle (1979; their Figure 11). (To understand this behavior, we note that the relaxation resulting from the strike-slip component of slip tends to negate that arising from the dip-slip component.) By including the contribution of the strike-slip component of the coseismic slip model, we may revise the viscosity estimate suitably to produce an optimal fit to the leveling data. We find that using the Ando (1971) source model, a revised viscosity of

$\eta=1.0\times 10^{19}$ Pa s produces a good fit to the leveling data (Figure 10b).

We calculate a forward model of the postseismic relaxation field from 1924 to 1931 using the distributed slip model of Pollitz et al. (2005) (Figure 2b) as the driving source. The viscoelastic parameters are $H_e=50$ km and $\eta=10^{19}$ Pa s. The resulting displacement field shown in Figure 11 is characterized by a broad depression west of Tokyo and a center of uplift just to the SW of the tip of the Boso Peninsula. The source model is similar to the uniform slip model used in Figure 8 (top), and the displacement fields shown in Figure 8 and Figure 11 are similar. The predicted vertical displacement on the Boso Peninsula (Figure 11) consists of maximum uplift at the southern tip of the Boso Peninsula and decreasing uplift towards the NE. This is contrary to what is observed (Figure 10, bottom). We find in additional tests that the tendency of landward tilt away from the southern tip is common to all models involving a shallow dip ($20\text{--}35^\circ$) of the PHS-Honshu interplate boundary and significant slip confined to the 0–25 km depth range. For example, these tests show that the tendency for postseismic landward tilt is exhibited for all uniform 1-plane coseismic models that dip less than 35° and have upper edge near the Sagami trough and a 2:1 ratio between strike-slip and dip-slip motions, regardless of fault length. A coseismic slip model involving a 45° interplate boundary, such as the Ando (1971) model, does produce oceanward tilt in the sense that qualitatively matches the observed leveling displacements along the Boso route (Figure 10b). Therefore, the primary factor controlling landward versus oceanward postseismic tilt of the Boso Peninsula from the viscoelastic relaxation process is the dip of the coseismic rupture plane.

In summary, whether or not viscoelastic relaxation of the sub-lithosphere is sufficient to explain the postseismic leveling observations along the Boso route rests upon the plausibility of the fault geometry. On the basis of seismicity, Ishida (1992) finds the dip of the PHS-Honshu slab interface to range from about 20 to 35° . Therefore, significant coseismic slip along a 45° -dipping interface is unlikely. Synthetic models using either uniform slip (Figure 8) or distributed slip (Figure 11) produce postseismic vertical displacement patterns that are contrary to the observed Boso leveling profile, and this compels us to search for an alternative mechanism to explain this profile.

3.2 Afterslip on the PHS slab interface

We explore whether postseismic afterslip along the coseismic rupture surface or its spatial extensions can reproduce the observed vertical displacement patterns. We first consider afterslip deeper than about 25 km, the maximum depth extent of significant slip in both uniform and distributed coseismic slip models (Nyst et al., 2005; Pollitz et al., 2005). We project potential afterslip planes along the deeper extension of coseismic rupture plane #1 (Figure 2a), assign a lower edge depth of 60 km, and assume uniform slip on afterslip planes with upper edge depths of 25, 32, and 42 km, respectively. The resulting fits to the Boso leveling profile are shown in Figure 12a. We find that the best fit to the data is achieved with an upper edge depth of 32 km, which associated with NRMS=2.50. (The initial rms misfit is 10.1) Although such a model conforms approximately to the observed postseismic leveling profile, the resulting uplift pattern does not adequately match the observed local maximum on the western Boso peninsula (profile distance 20 km) or local minimum on the southern Boso peninsula (profile distance 80 km), and is too smooth to match the sharp minimum on the southern Boso peninsula.

We further consider deep afterslip planes which do not necessarily lie on the downdip extension of the coseismic rupture plane. We generate a suite of models in which the length and rake of the hypothetical afterslip plane are fixed at 90 km and 135° , respectively, and the lower edge is constrained to lie below the surface projection of the line segment represented by the intersection of the deeper plane #1 extension (Figure 2a) with an arbitrary depth isosurface, which we take to be the 60-km depth surface. A search is performed over the parameters $\{d_{\max}, d_{\min}, \delta, u\}$ which denote {lower edge depth, upper edge depth, dip, slip} associated with the afterslip. The resulting grid search is performed over 1848 such models sampling lower edge depths ranging from 60 to 115 km, upper edge depths from 20 to 48 km, and dip from 22° to 48° . (Slip is inverted explicitly in each realization of the other three parameters.) The best such model is associated with $d_{\max}=100$ km, $d_{\min}=30$ km, $\delta=46^\circ$, and $u=32.5$ cm; the associated NRMS is 2.01. Figure 12b shows the pattern of NRMS as a function of δ and d_{\min} (d_{\max} being held fixed at 100 km) and the resulting fit to the Boso leveling profile. Figure 12c shows the corresponding patterns for the case $d_{\max}=80$ km, which possesses a minimum NRMS of 2.03 at $d_{\min}=30$ km, $\delta=38^\circ$, and $u=34.6$ cm. Although NRMS at the respective minima in these cases are smaller than those in which the afterslip plane is constrained to lie in the coseismic rupture plane,

the resulting predicted leveling pattern is of much longer wavelength than observed, and the area of maximum subsidence is invariably ~ 20 km north of the observed maximum subsidence.

A model of shallow afterslip is found to provide a qualitatively better fit to the postseismic Boso leveling profile than any of the previously considered models. We perform a trial-and-error search for the geometry and slip of afterslip planes constrained to have an upper edge at Earth's surface and a lower edge depth within the upper 20 km, and to lie on coseismic rupture plane #1 or its spatial extension(s). The best such afterslip plane found by this procedure is plane #4 in Figure 3. This plane and its slip sense and relation to the coseismic slip distribution is shown in Figure 2b. It corresponds to 127 cm of oblique afterslip (rake = 160°) along a 55 km-long, N46°W-striking, 23°-dipping plane extending from 0 to 12.8 km depth. We consider the corresponding vertical motion and its possible combination with a viscoelastic relaxation signal in the Boso peninsula leveling profile. A comparison of these predicted uplifts with the observed uplift is shown in Figure 13a. The corresponding NRMS values are: 2.22 (shallow afterslip alone), 3.22 (relaxation alone), and 1.77 (combined shallow afterslip plus relaxation). This comparison reveals that: (1) both viscoelastic relaxation of the sub-lithosphere and shallow afterslip are consistent with the observed Boso peninsula leveling, (2) a model of shallow afterslip matches the main features of the data (particularly the sharp minimum on the southern Boso peninsula), and (3) a model of combined shallow afterslip and viscoelastic relaxation provides the best fit to the data. Although both processes appear to contribute to postseismic deformation on the Boso peninsula, the relative performance between the afterslip-alone case and relaxation-alone case nevertheless suggests a minor role for viscoelastic relaxation beneath the Boso peninsula after the 1923 earthquake.

3.3 Non-PHS afterslip?

A large north-south horizontal contraction is observed in the Mitaka region just west of Tokyo during the first year postseismic period, as seen in the e_{22} component of the strain field deduced from the Mitaka Rhombus (Figure 5). The $\sim 10\mu$ strain amplitude of this signal, the comparable amplitude of subsequent fluctuations in the e_{22} and e_{11} strains, as well as the existence of at least one reversal in deformation sense from

1923 to 1980, cannot be explained with a model of postseismic mantle relaxation. For example, a model of postseismic mantle relaxation ($H_e=50$ km and $\eta=1.4\times 10^{19}$ Pa s) is found to exhibit a monotonic time-dependence in all strain components and amplitudes about 10 times smaller than what is observed. Thatcher and Fujita (1984) explained the rapid postseismic strain evolution from 1923/9 to 1924/8 (September, 1923 to August, 1924) in terms of a model of deep afterslip. We have reconstructed the afterslip plane used in that study (Figure 14) and assigned identical dislocation parameters, i.e., 1 meter of slip on the downdip extension of the Ando (1974) rupture plane, with a 2:1 ratio in right-lateral strike-slip to dip-slip motion. The resulting strain values are: $e_{22}=-2.21$ μ strain, $e_{11}=-0.36$ μ strain, and $e_{12}=-0.87$ μ strain. This is approximately a factor of 5 less than the result of the identical calculation in Thatcher and Fujita (1984) as well as the observation. If we assume that the present calculations are being performed correctly, then about 5 meters of slip would satisfactorily explain the 1923/9 - 1924/8 strain evolution at Mitaka. However, the same dislocation model also predicts from ~ 0 up to 27 cm uplift on the postseismic Tokyo-Atami leveling route, which is much larger than the variations in postseismic vertical displacement that were observed (Figure 3b). (Since the first-epoch postseismic leveling observations on the northern half of the Tokyo-Atami line were performed in 1923/12, one would expect most of the dislocation signal to be captured in these leveling measurements.)

It is possible that the 1923/9 to 1924/8 strain changes could arise from poroelastic rebound of the uppermost crust following the 1923 earthquake. Near-surface coseismic dilatation $e_{11}+e_{22}$ is ~ 30 μ strain in the Mitaka region (Figure 5), and postseismic contractile strain would be expected as a result of postseismic poroelastic flow. Such behavior is consistent with the observed postseismic movements around the 1992 Landers rupture zone in the first few months following the Landers earthquake (Peltzer et al., 1996). However, the 1924/9 to 1924/8 dilatation observed at Mitaka is ~ 12 μ strain, and the difference in dilatation between the drained and undrained states is found to be of order ~ -0.1 μ strain for Poisson's ratios of 0.31 (undrained) and 0.27 (drained). This is 2 orders of magnitude too small to explain the observed dilatation change. Differences between postseismic e_{11} and e_{22} could possibly be attributed to calibration errors in the short range EDM instrument used to measure the line lengths in the Mitaka rhombus.

A trial-and-error search is performed over a suitable range of possible dislocation planes which are constrained to lie in the downdip or lateral extension of the principal coseismic ruptures planes (planes #1, 2 in Figure 3), with slip sense constrained to have rake ranging from 90° to 153° . Thus all considered models involve thrust motion on NE-dipping faults. We find that no such dislocation model satisfactorily explains the Mitaka strain data and the Tokyo-Atami postseismic leveling data simultaneously. In one set of cases, the sign and amplitude of the horizontal strains at Mitaka are correctly obtained, but an unacceptably large perturbation on the Tokyo-Atami line is predicted. In all other cases, the sign of the e_{22} change at Mitaka is incorrect. This leads us to consider other afterslip-dislocation models involving dominantly thrust motion on NE-dipping planes or normal faulting on SW-dipping planes. We find solutions of both types that satisfy the observed horizontal strain changes at Mitaka. A normal faulting solution would be associated with large coseismic Coulomb stress changes (from the main 1923 rupture) and would therefore be encouraged by the coseismic rupture. However, such a solution is inconsistent with the overall tectonic regime. A satisfactory thrust faulting solution, involving 3.1 meters of dominantly dip-slip motion, is shown as the "Western afterslip plane" in Figure 14. It also satisfies the Mitaka strain data with an effect on the Tokyo-Atami leveling line not exceeding 2.5 cm. This solution is associated with positive coseismic Coulomb stress change on part of the afterslip plane (Figure 14), so that it could have been active immediately after the main coseismic rupture. If such afterslip in this locality did indeed occur, then it was not accompanied by aftershock activity.

4 Discussion

The role of viscoelastic relaxation in explaining postseismic deformation measurements after the 1923 earthquake is apparently minor or nonexistent near the Boso peninsula, but it appears important beneath mainland Honshu. This is based on a search for the parameters of a viscoelastic model capable of explaining the Tokyo-Atami postseismic uplift pattern. Using the data in Figure 3 we performed a grid search for the parameters H_e and η which produce the best fit to the Tokyo-Atami leveling profile. The residual misfit as a function of η for various values of H_e is shown in Figure 15. Although the fits with relatively small η and $H_e=60$ are slightly better

than those obtained with other choices of H_e , these parameters are clearly not well resolved. A relatively low viscosity of 5×10^{18} Pa s and $H_e \geq 50$ km is suggested by these fits. However, if $\eta = 5 \times 10^{18}$ Pa s and $H_e = 50$ or 60 km, the resulting vertical deformation pattern from 1924 to 1931 is associated with maximum subsidence of 25 cm centered about 75 km west of Tokyo, and from 1931 to 1950 it is associated with additional maximum subsidence of 15 cm in the same location. This is much larger than observed subsidence from 1931 to 1950 (Dambara and Hirobe, 1964), and therefore we prefer a somewhat larger value of η . For concreteness we choose the values $H_e = 50$ km and $\eta = 1.4 \times 10^{19}$ Pa s for further consideration. A mantle viscosity value near 10^{19} Pa s is consistent with that estimated in other regions of Japan (e.g., Miyashita, 1987; Rydelek and Sacks, 1988). The fit of the corresponding viscoelastic model to the leveling data is shown in Figure 13b, together with the fits of the shallow-afterslip model and the combined afterslip and relaxation model. Clearly the afterslip source near the Boso peninsula would contribute little to the deformation, but the viscoelastic model reproduces the main feature of the observed leveling profile, the broad relative minimum in uplift about midway between Tokyo and Atami. This is consistent with the pattern shown in Figure 9 for a slightly different viscoelastic structure. Figure 13a and 14b together show that the occurrence of both shallow off-Boso afterslip and viscoelastic relaxation at least beneath mainland Honshu, and possibly beneath the Boso peninsula, is consistent with available deformation constraints.

The combined afterslip plus viscoelastic relaxation model is further consistent with the postseismic subsidence recorded at the Aburatsubo tide gage station (Figure 4). The predicted subsidence from 1924 to 1931 in the combined model is 5.0 cm, of which 4.3 cm is contributed by the afterslip source and 0.7 cm is contributed by viscoelastic relaxation (with $H_e = 50$ km and $\eta = 2 \times 10^{19}$ Pa s). This is in reasonable agreement with the observed 4.2 cm subsidence over this postseismic time period as derived from the tide gage record in section 3.

Recent investigation into the interseismic loading behavior of the PHS-Honshu and Pacific-Honshu interplate boundaries (Nishimura and Sagiya, 2005) reveals that the part of the PHS-Honshu boundary to the S and SE of the Boso peninsula is nearly fully locked and rapidly accumulating strain. The coseismic distributed slip model (Figure 2b) yields from 1 to 2 meters slip in this region, though little coseismic slip is

detected further east than about 139.9°E . Thus much of the offshore portion of the PHS- Honshu interplate boundary apparently remains at a slip deficit. This is difficult to constrain because the relevant geodetic observations are obviously limited to the land regions and would therefore have difficulty resolving possible coseismic slip further east. However, if that portion last ruptured in the 1703 earthquake, then at a backslip rate of ~ 3 cm/yr a potential slip of 9 meters would be stored (Pollitz et al., 1996). Of this, perhaps 1 m was relieved by the inferred shallow afterslip following the 1923 event, so that about 8 m potential slip would remain.

The models of postseismic processes derived here provide a basis for calculating postseismic stress evolution following the 1923 earthquake. For this purpose we assume the distributed coseismic slip model (Figure 2b) and the rheological model ($H_c=50$ km, $\eta=1.4\times 10^{19}$ Pa s) that best fit the Tokyo-Atami leveling line. We calculate the coseismic and accumulated viscoelastic-model and interseismic-model (from 1923 to 2000) strain field at a depth of 15 km. The interseismic model component is calculated according to the backslip model presented by Nishimura and Sagiya (2005). We then calculate the change in Coulomb failure stress ΔCFS (e.g., King et al., 1994) on receiver fault planes with fixed geometry and slip. Figure 16 shows ΔCFS on receiver planes with geometry and slip similar to the main rupture of the 1923 earthquake. Lobes of positive coseismic ΔCFS (Figure 16a) are concentrated in the southern Boso peninsula and especially west of the small coseismic rupture plane (northern Izu peninsula), amounting to several bars. These local maxima are well correlated with the occurrence of crustal aftershocks of the Kanto earthquake (Figure 16a). Negative coseismic ΔCFS is concentrated over a broad area to the north and south of the coseismic rupture planes. Maximum ΔCFS due to viscoelastic relaxation is 4 to 5 bars centered in the area of central Tokyo Bay (Figure 16b), within the area of the coseismic rupture planes, extending westward across the northern Izu peninsula where it constructively interferes with the coseismic ΔCFS . A lesser amount of constructive interference occurs also in the central Boso peninsula. The interseismic-model stress change (Figure 16c) tends to counteract the coseismic stress change and re-stress those areas which had undergone a stress decrease in 1923.

Focal mechanisms of recent crustal seismicity delineate distinct groups of epicenters, each associated with a definite horizontal stress field (Figure 17). The group located north of the Izu peninsula at about 35.5°N is associated with a NW-SE

principal axis of compression and thrust faulting, while the group to the east the Izu peninsula between 34.8°N and 35.0°N is associated with a NW-SE principal axis of compression and strike-slip faulting. The latter cluster of epicenters is near a proposed tear in the Philippine Sea Plate, the West Sagami Bay Fracture (WSBF -- Ishibashi, 1988; Koyama and Umino, 1991). The focal mechanism solutions are consistent with left-lateral faulting on a north-striking WSBF, but the NW-SE trend of the epicenters is discordant with any north-striking structure. Thus these earthquakes cannot be considered to occur on a single fault. The sequences of seismicity in this region have a swarm-type behavior, and geodetic studies suggest active dike opening (e.g., Okada and Yamamoto, 1991; Aoki et al., 1999). East of the Izu peninsula and south of 34.8°N, the intense seismic activity (Figure 17) is associated with volcanic sources with highly variable focal mechanisms.

Patterns of stress changes resulting from combined coseismic effects, postseismic relaxation, and interseismic strain accumulation for two different time periods are shown in Figure 18. The receiver fault geometry corresponds to reverse faulting on planes with fixed strike=315°, dip=30°, and rake=153°. Comparison of Figure 18b for the 1923-2000 time period with Figure 17 indicates a good correlation of the occurrence of recent crustal seismicity with predicted lobes of Δ CFS in the region north of the Izu peninsula around 35.5°N, 139.0°E. A negative correlation occurs just east of the Izu peninsula around latitude 34.8°N to 35.0°N. Assuming that these events are associated with left-lateral strike-slip faulting on locally north-striking faults, we may calculate Δ CFS assuming this receiver geometry (fixed strike=0°, dip=90°, and rake=0°). Figure 19 shows the resulting Δ CFS pattern together with the epicenters of shallow crustal earthquakes from 1979 to 1996. In the region between 34.8°N and 35.0°N there is an excellent correlation of seismicity with positive Δ CFS of several bars. This suggests that the occurrence of these earthquakes has been assisted by the stress changes accompanying the 1923 earthquake. The 1923 effects and subsequent interseismic loading may reinforce the stressing of the WSBF from inflation beneath the Izu Peninsula, as proposed by Thatcher and Savage (1982). Considering the different tectonic regimes in the region (N to NE directed thrusting in the area north of Izu peninsula; left-lateral strike-slip faulting in the area east of the Izu peninsula), the manifestations of 1923 earthquake-related stress changes were evident immediately after the earthquake and persist in seismicity patterns six to seven

decades after the earthquake.

Stress increases would also be predicted along the down-dip extension of the PHS plate beneath the maximum depth ~ 25 km of the coseismic rupture. Although part of this stress increase could be accommodated by afterslip, the lack of deep afterslip following the 1923 earthquake (section 3.2) implies that such stress increases would need to be accommodated elsewhere during the seismic cycle. Bakun (2005) has suggested that slippage associated with the destructive 1855 Ansei-Edo earthquake occurred along the down-dip extension of the PHS plate, which would imply that, at least during the most recent earthquake sequence, 1855-type events eventually lead to 1923-type events rather than vice-versa.

5 Conclusions

Consideration of available postseismic deformation data in the ~ 8 years following the 1923 earthquake, combined with a newly-derived slip model of the 1923 main event, yields new insights into the processes that were active during the early postseismic epoch. Although the amount of data available to describe the postseismic epoch is very limited compared with that available to constrain the coseismic rupture, they are sufficient to identify the main processes to first order. The dominant postseismic processes are inferred to be: (1) broadscale viscoelastic relaxation of a ~ 50 km-thick stratified elastic mechanical lithosphere overlying a viscoelastic substrate (assumed isoviscous) of viscosity of $1 - 2 \times 10^{19}$ Pa s, and (2) afterslip along a shallow, $\sim 23^\circ$ -dipping plane offshore and SW of the Boso peninsula. These two processes are consistent with available postseismic leveling and tide gage measurements collected in the first ~ 8 years following the 1923 earthquake. Additional processes such as afterslip inland (not on the PHS slab interface) may be necessary to explain very large strain changes recorded at a small-aperture EDM array west of Tokyo (Mitaka Rhombus).

Stress changes associated with the 1923 earthquake and associated relaxation have been derived from the distributed coseismic slip model presented in Pollitz et al. (2005). If account is taken for the different tectonic regimes that characterize the region, then coseismic and subsequent post-1923 stress changes are consistent with earthquake activity in the region even eight decades after the earthquake. The

occurrence of seismicity associated with thrust faulting north of the Izu peninsula, together with the absence of such faulting in the region north of Sagami Bay and west of Tokyo, is consistent with the predicted Coulomb stress pattern. Similarly, the occurrence of seismicity associated with strike-slip faulting east of the Izu peninsula, is consistent with the predicted Coulomb stress pattern. Although our simple model ignores lateral variations in viscosity which certainly must arise due to the complicated plate configuration, it appears sufficiently detailed to capture the main features of the early postseismic deformation as well as the long-lived stress field.

Acknowledgments. We are grateful to Shinji Toda, Takeshi Sagiya, and Ross Stein for helpful discussions, and Serkan Bozkurt for assistance with graphics. We thank two anonymous reviewers and the Associate Editor for constructive criticisms which helped improve this paper. We thank Shinki Toda for providing the original version of Figure 17.

References

- Ando, M., A fault-origin model of the Great Kanto earthquake of 1923 as deduced from geodetic data, *Bull. Earthq. Res. Inst.*, 49, 19-32, 1971.
- Aoki, Y., and C.H. Scholz, Vertical deformation of the Japanese islands, 1996-1999, *J. Geophys. Res.*, 108, 2257, doi: 10.1029/2002JB002129, 2003.
- Aoki, Y., P. Segall, T. Kato, P. Cervelli, and S. Shimada, Imaging magma transport during the 1997 seismic swarm off the Izu Peninsula, Japan, *Science*, 286, 927-930, 1999.
- Bakun, W.H., Magnitude and location of historical earthquakes in Japan and implications for the 1855 Ansei Edo earthquake, *J. Geophys. Res.*, *in press*, 2005.
- Barbosa, S.M., M.J. Fernandes, and M.E. Silva, Nonlinear sea level trends from European tide gauge records, *Annales Geophysicae*, 22, 1465-1472, 2004.
- Dambara, T., and M. Hirobe, Vertical movements of Japan during the past 60 years, II. Southern part of the Kanto district, *J. Geod. Soc. Jpn.*, 10, 61-70, 1964.
- DeMets, C., R.G. Gordon, D.F. Argus, and S. Stein, Current plate motions, *Geophys. J. Int.*, 101, 425-478.
- Heki, K., S. Miyazaki, H. Takahashi, M. Kasahara, F. Kimata, S. Miura, N. Vasilenco, A. Ivashchenko, and K. An, The Amurian plate motion and current plate kinematics in Eastern Asia, *J. Geophys. Res.*, 104, 29,147-29,155, 1999.
- Ishibashi, K., 'Kanagawa-ken-seibu Earthquake' and earthquake prediction II, *Kagaku*, 58, 771-780, 1988. (In Japanese.)
- Ishida, M., Geometry and relative motion of the Philippine Sea plate and Pacific plate beneath the Kanto-Tokai district, Japan, *J. Geophys. Res.*, 97, 489-513, 1992.
- Koyama, M., and S. Umino, Why does the Higashi-Izu monogenetic volcanic group exist in the Izu peninsula?: Relationships between Late Quaternary volcanism and tectonics in the northern tip of the Izu-Bonin arc, *J. Phys. Earth*, 39, 391-420, 1991.
- King, G.C., R.S. Stein, and J. Lin, Static stress changes and the triggering of earthquakes, *Bull. Seism. Soc. Am.*, 84, 935-953, 1994.
- Matsu'ura, M., and T. Iwasaki, Study on coseismic and postseismic crustal movements associated with the 1923 Kanto earthquake, *Tectonophysics*, 97, 201-215, 1983.
- Mazzotti, S., P. Henry, X. Le Pichon, Transient and permanent deformation of central

- Japan estimated by GPS 2. Strain partitioning and arc-arc collision, *Earth Planet Sci. Lett.*, 184, 455-469, 2001.
- Military Land Survey, Re-survey of the Kwanto district after the great earthquake of 1923, *Bull. Imp. Earthq. Invest. Comm.*, 11, 1-6, 1930.
- Miyashita, K., A model of plate convergence in southwest Japan, inferred from leveling data associated with the 1946 Nankaido earthquake, *J. Phys. Earth*, 35, 449-467, 1987.
- Nakamura, K., Possible nascent trench along the eastern Japan Sea as the convergent boundary between Eurasian and North American plates, *Bull. Earthq. Res. Inst. Univ. Tokyo*, 58, 711-722, 1983.
- Nishimura, T., and T. Sagiya, Crustal block kinematics around the northernmost Philippine Sea plate, central Japan estimated from GPS and Leveling data, *J. Geophys. Res.*, in preparation, 2005.
- Nyst, M., T. Nishimura, N. Hamada, F.F. Pollitz, and W. Thatcher, The 1923 Kanto Earthquake re-evaluated using a newly augmented geodetic data set, *J. Geophys. Res.*, submitted, 2005.
- Okada, Y., and E. Yamamoto, Dike intrusion model for the 1989 seismovolcanic activity off Ito, central Japan, *J. Geophys. Res.*, 96, 10361-10176, 1991.
- Peltzer, G., P. Rosen, F. Rogez, and K. Hudnut, Postseismic rebound in fault steps caused by pore fluid flow, *Science*, 273, 1202-1204, 1996.
- Pollitz, F.F., M. Nyst, and T. Nishimura, Coseismic slip distribution of the 1923 Kanto earthquake, *J. Geophys. Res.*, accepted, 2005.
- Pollitz, F.F., X. Le Pichon, and S. Lallemand, Shear partitioning near the central Japan triple junction: the 1923 great Kanto earthquake revisited-II, *Geophys. J. Int.*, 126, 882-892, 1996.
- Pollitz, F.F., Gravitational-viscoelastic postseismic relaxation on a layered spherical Earth, *J. Geophys. Res.* 102, 17,921-17,941, 1997.
- Rydelek, P.A., and I.S. Sacks, Asthenospheric viscosity inferred from correlated land-sea earthquakes in north-east Japan, *Nature*, 336, 234-237, 1988.
- Sagiya, T., Interplate coupling in the Kanto district, central Japan, and the Boso peninsula silent earthquake in May 1996, *Pure Appl. Geophys*, 161, 2327-2342, 2004.
- Sato, T., R.W. Graves, P.G. Somerville, and S. Kataoka, Estimates of regional and local strong motions during the Great 1923 Kanto, Japan, earthquake (Ms 8.2).

- Part 2: Forward simulation of seismograms using variable-slip rupture models and estimation of near-fault long-period ground motions, *Bull. Seismol. Soc. Am.*, 88, 206-227, 1998.
- Seno, T., T. Sakurai, and S. Stein, Can the Okhotsk plate be discriminated from the North American plate?, *J. Geophys. Res.*, 101, 11,305-11,315, 1999.
- Thatcher, W., and N. Fujita, Deformation of the Mitaka Rhombus: Strain buildup following the 1923 Kanto earthquake, central Honshu, Japan, *J. Geophys. Res.*, 89, 3102-3106, 1984.
- Thatcher, W., and J.C. Savage, Triggering of large earthquakes by magma chamber-inflation, Izu peninsula, Japan, *Geology*, 10, 637-640, 1982.
- Thatcher, W., and J.B. Rundle, A model for the earthquake cycle in underthrust zones, *J. Geophys. Res.*, 84, 5540-5556, 1979.
- Yoshioka, S., T. Yabuki, T. Sagiya, T. Tada, and M. Matsu'ura, Interplate coupling in the Kanto district, central Japan, deduced from geodetic data inversion and its tectonic implications, *Tectonophysics*, 229, 181-200, 1994.

Figure Captions

Figure 1. Tectonic setting of Kanto and Tokai districts indicating major tectonic boundaries. PHS=Philippine Sea plate; PAC=Pacific plate; N.AMER=North American plate; AMUR=Amurian plate; ISTL=Itoigawa-Shizuoka Tectonic Line.

Figure 2. (a) Locations of two postseismic leveling lines (red dots), tide station Aburatsubo (labelled "Ab.") and Mitaka Rhombus strain array. Fault planes #1, 2, and 3 are used to characterize the distributed slip model of the 1923 earthquake (b), and plane #4 is a shallow afterslip plane inferred to have accommodated slip during the first 8 years postseismic time interval. (b) Distributed coseismic slip model presented in Pollitz et al. (2005), derived from triangulation and leveling data. Amplitude and slip directions on the hanging wall are indicated for inter-plate boundary faults #1 and #2. together with right-lateral slip value of fault #3 (Boso transform). The Boso transform is a vertical fault with upper and lower edge depths of 2 km and 15 km, respectively, associated with about 40 cm right-lateral strike-slip motion. Also shown is the geometry and slip sense of a shallow afterslip plane, derived by a process of trial-and-error, inferred by fitting postseismic leveling data.

Figure 3. Cumulative displacement measured across the Boso and Tokyo-Atami leveling lines from 1923-1931 and 1923-1930, respectively. Profile locations indicated in Figure 2a.

Figure 4. Sea level height measurements made at tide station Aburatsubo (Figure 2a) since 1896. Beset-fitting straight line fits are indicated for the time periods 1924-1931 and 1950-2000, yielding rates of 8.2 mm/yr and 2.2 mm/yr. If the latter is considered the background sea level change rate, then the tectonic motion inferred at Aburatsubo from 1924 to 1931 amounts to 4.2 cm subsidence.

Figure 5. Time series of horizontal tensor strain (tensile strain positive) recorded in the Mitaka rhombus (see Figure 2a for location) from 1916 to 1980. Vertical bars indicate one standard deviation in the measurement. (From Figure 2 of Thatcher and Fujita, 1984.)

Figure 6. Schematic description of postseismic processes active following the 1923 earthquake. The mechanical parameters in the viscoelastic-relaxation case

are the elastic plate thickness H_e and mantle viscosity η .

Figure 7. Distribution of elastic parameters in 1D Earth model (Sato et al., 1998) and delineation of elastic and viscoelastic regions.

Figure 8. Calculated displacement field of postseismic relaxation during the first 8 years following the 1923 earthquake, calculated using the indicated parameters. The only difference between the two cases is the dip of the fault (23° or 45° towards the right of the plot).

Figure 9. Calculated displacement field of postseismic relaxation during the first 8 years following the 1923 earthquake, calculated using the Ando (1971) fault geometry and slip and mechanical parameters $H_e=60$ km, $\eta=6\times 10^{19}$ Pa s.

Figure 10. Comparison of Boso and Tokyo-Atami cumulative postseismic displacements with predictions of Ando (1971) model, using (a) $\eta=6\times 10^{19}$ Pa s or (b) $\eta=10^{19}$ Pa s. NRMS is the normalized root-mean-square misfit defined by equation (1).

Figure 11. Surface postseismic displacement field from 1924 to 1931 calculated on the Earth model with $H_e=50$ km and $\eta=10^{19}$ Pa s. The source model is the coseismic distributed slip model (Figure 2b).

Figure 12. Predictions of deep-afterslip models and comparison with observed leveling data along the Boso peninsula profile. (a) All considered afterslip planes lie along the extension of coseismic rupture plane #1 and are assigned lower edge depth of 60 km, rake of 135° , and slip of 0.5 m. The different subplots correspond to different locations of the upper edge. NRMS is the normalized root-mean-square misfit defined by equation (1). (b) Considered afterslip planes are constrained to have identical length, rake, and surface projection of the lower edge (see text), but lower edge depth d_{\max} , upper edge depth d_{\min} , dip δ , and slip u are considered variable. The upper figure shows the variation of NRMS with δ and d_{\min} for fixed $d_{\max}=100$ km. Afterslip magnitude is inverted for each realization of δ and d_{\min} . The black dot indicates the upper edge and dip values associated with minimum NRMS for the given d_{\max} . The lower figure shows the resulting fit to the Boso leveling profile. (c) Same as (b) but with fixed $d_{\max}=80$ km.

Figure 13. Predictions of shallow-afterslip model (plane #4 in Figure 2a) and viscoelastic relaxation model and their sum, as compared with observed postseismic uplift on the (a) Boso peninsula and (b) Tokyo-Atami leveling profiles. NRMS is the normalized root-mean-square misfit defined by equation (1).

Figure 14. Geometry of Ando (1974) rupture plane and deep afterslip plane used by Thatcher and Fujita (1984) to model postseismic horizontal strain observations at Mitaka. Geometry and dislocation parameters are as follows: length=85 km, width=30 km, dip=30°, upper and lower edge depths=25 km and 40 km, respectively, slip=1.0 m (0.9 m right-lateral strike slip, 0.45 m dip slip). The plane labelled "Western afterslip plane" is one found to produce an adequate fit to the 1923/9 - 1924/8 postseismic horizontal strain changes at Mitaka. It has lower and upper edge depths of 13 km and 6 km, respectively, dips 30° toward the NE and has slip of 3.1 meters and rake 115°. This dislocation model predicts the following strains: $e_{11}=-3.7 \mu\text{strain}$, $e_{22}=-10.0 \mu\text{strain}$, $e_{12}=-3.4 \mu\text{strain}$. The coseismic Coulomb stress change on the proposed afterslip plane is shown, calculated by assuming fixed receiver fault geometry and an effective friction coefficient of 0.6.

Figure 15. Residual misfit of leveling data along the Atami-Tokyo line as a function of mantle viscosity for fixed $H_e=40, 50,$ and 60 km.

Figure 16. Coseismic (a), accumulated viscoelastic-model (1923 to 2000) (b), and accumulated interseismic-model (1923-2000) (c) change in normal stress, shear stress, and Coulomb failure stress, at depth 15 km, on receiver faults with fixed strike=315°, dip=30°, and rake=153°. An effective coefficient of friction of 0.4 is assumed. A contour interval of 1 bar is used to highlight positive stress changes. The input source model is the distributed slip model of Figure 2b (with Boso transform slip excluded), and the rheology parameters used are $H_e=50$ km and $\eta=1.4 \times 10^{19}$ Pa s. Grey planes indicated the boundaries of the two fault planes used in the distributed slip model. Superimposed on the coseismic Coulomb stress change in (a) are epicenters of aftershocks of depth less than 30 km occurring during the first month after the Kanto earthquake (Hamada et al., 2001).

Figure 17. Focal mechanism solutions of recent crustal earthquakes and delineation of groups of epicenters, each associated with a definite horizontal stress field.

For each group, the principal axis of compression is indicated with the arrows.

Figure 18. Coseismic plus accumulated viscoelastic-model and interseismic-model change in normal stress, shear stress, and Coulomb failure stress, at depth 15 km, from 1923-1950 (a) or 1923-2000 (b), on receiver faults with fixed strike= 315° , dip= 30° , and rake= 153° . Other conventions as in Figure 16.

Figure 19. Coseismic plus accumulated viscoelastic-model and interseismic-model change in normal stress, shear stress, and Coulomb failure stress, at depth 15 km, from 1923-2000 on receiver faults with fixed strike= 0° , dip= 90° , and rake= 0° . Epicenters of all $M \geq 4$ crustal earthquakes (depth ≤ 20 km), as obtained from the NEID catalog between 1979 and 1996, are superimposed. Other conventions as in Figure 16.

Figure 1

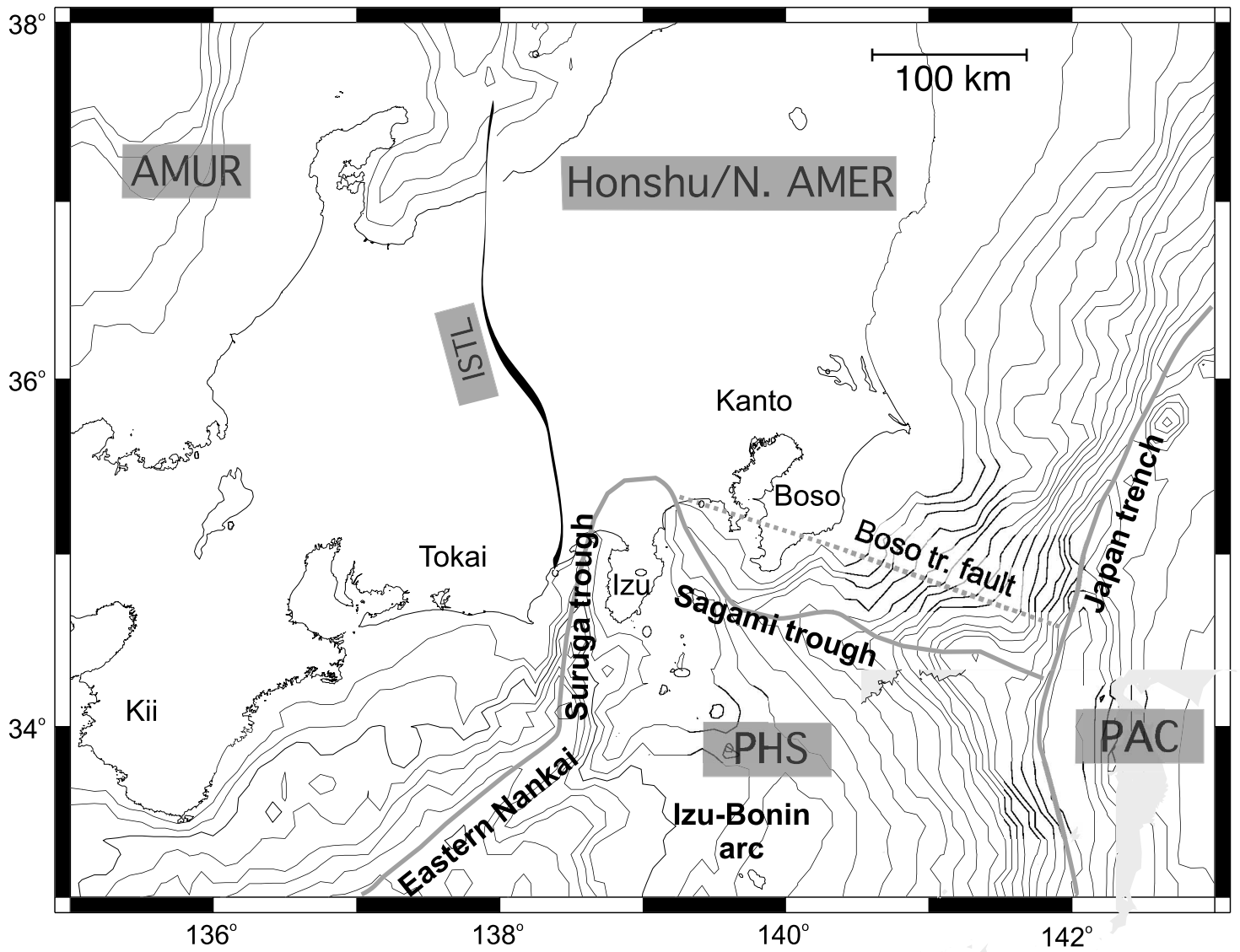


Figure 2

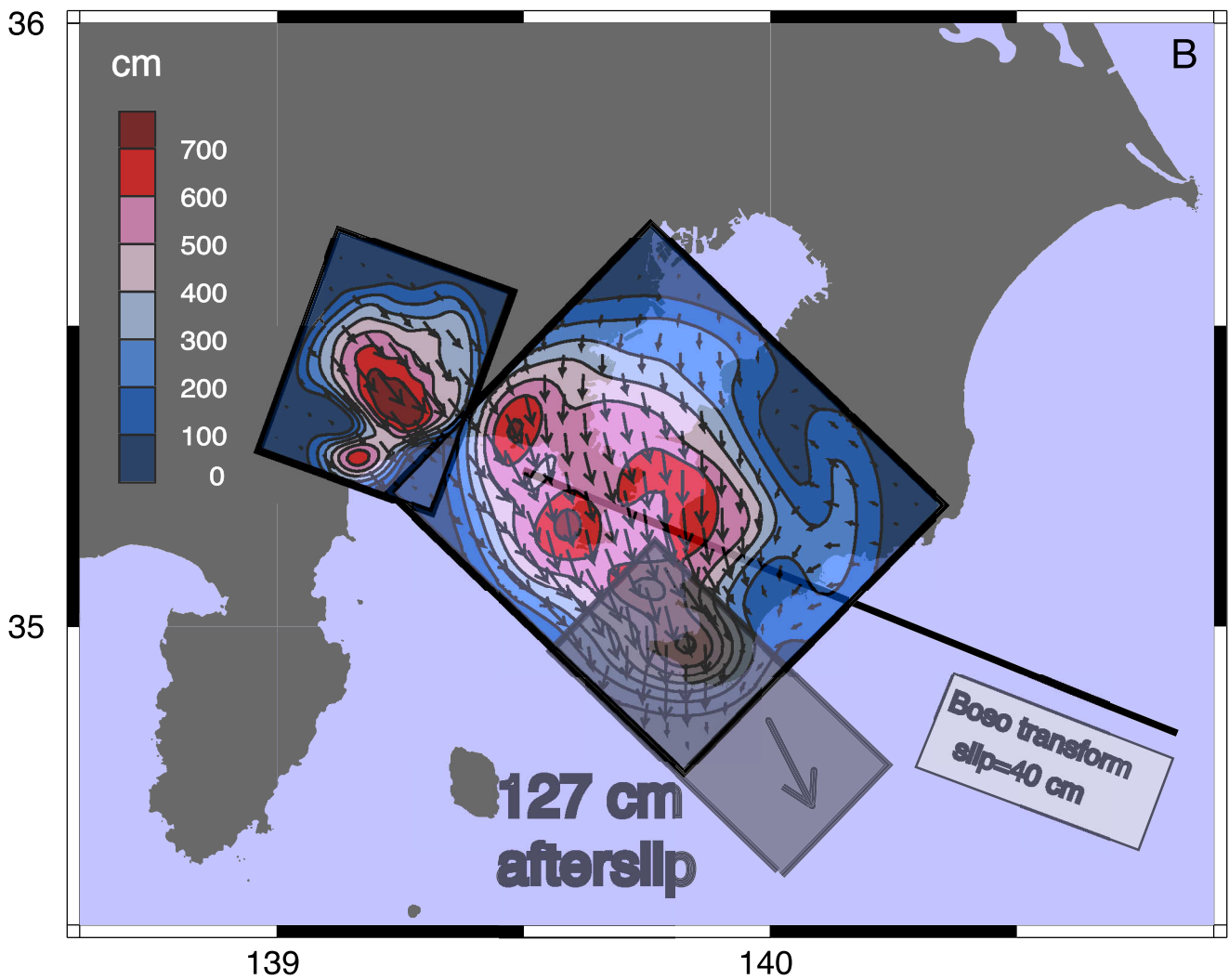
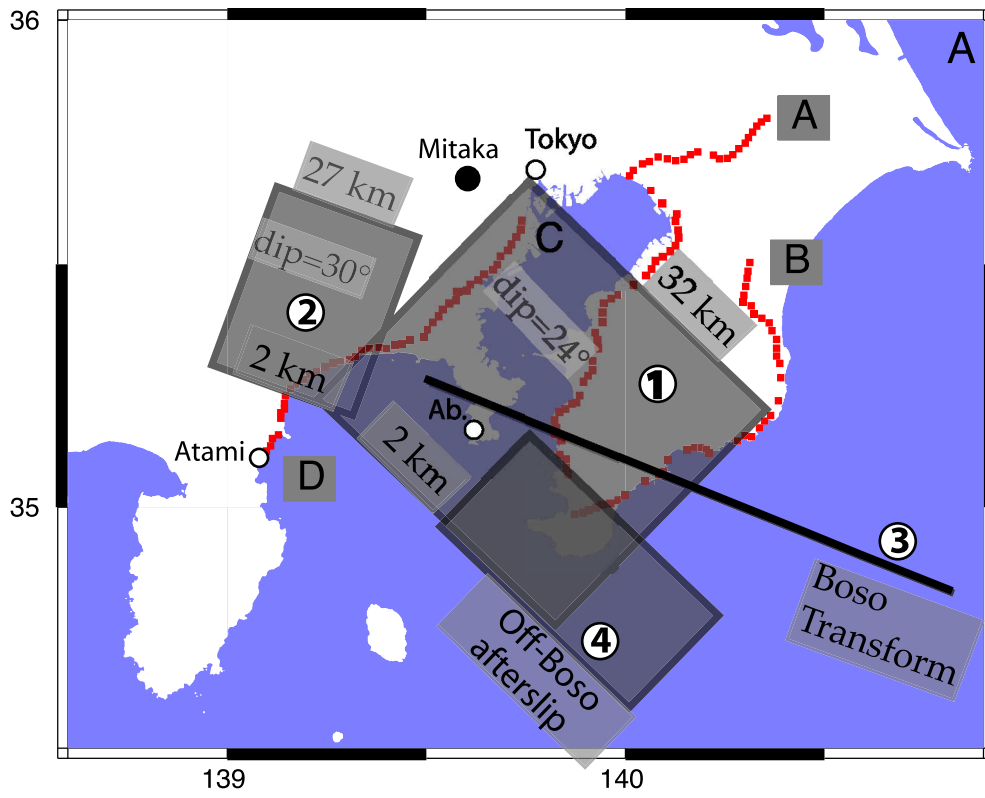


Figure 3

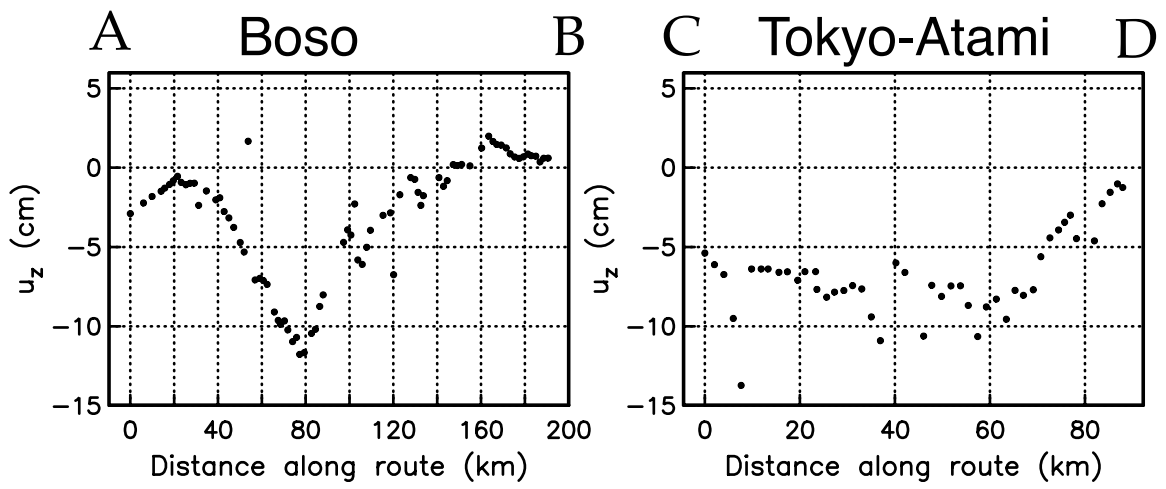


Figure 4

Aburatsubo tide gage

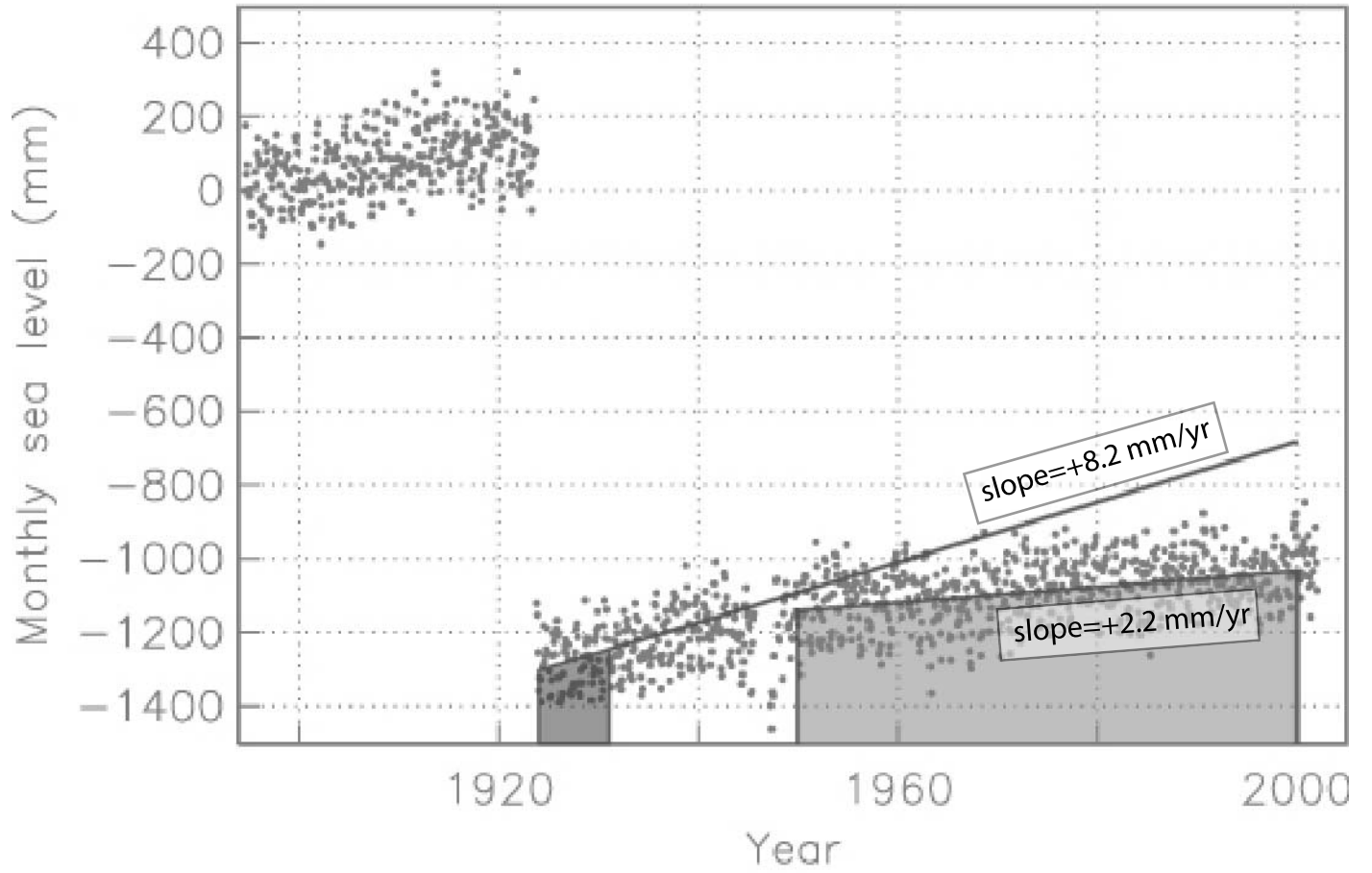
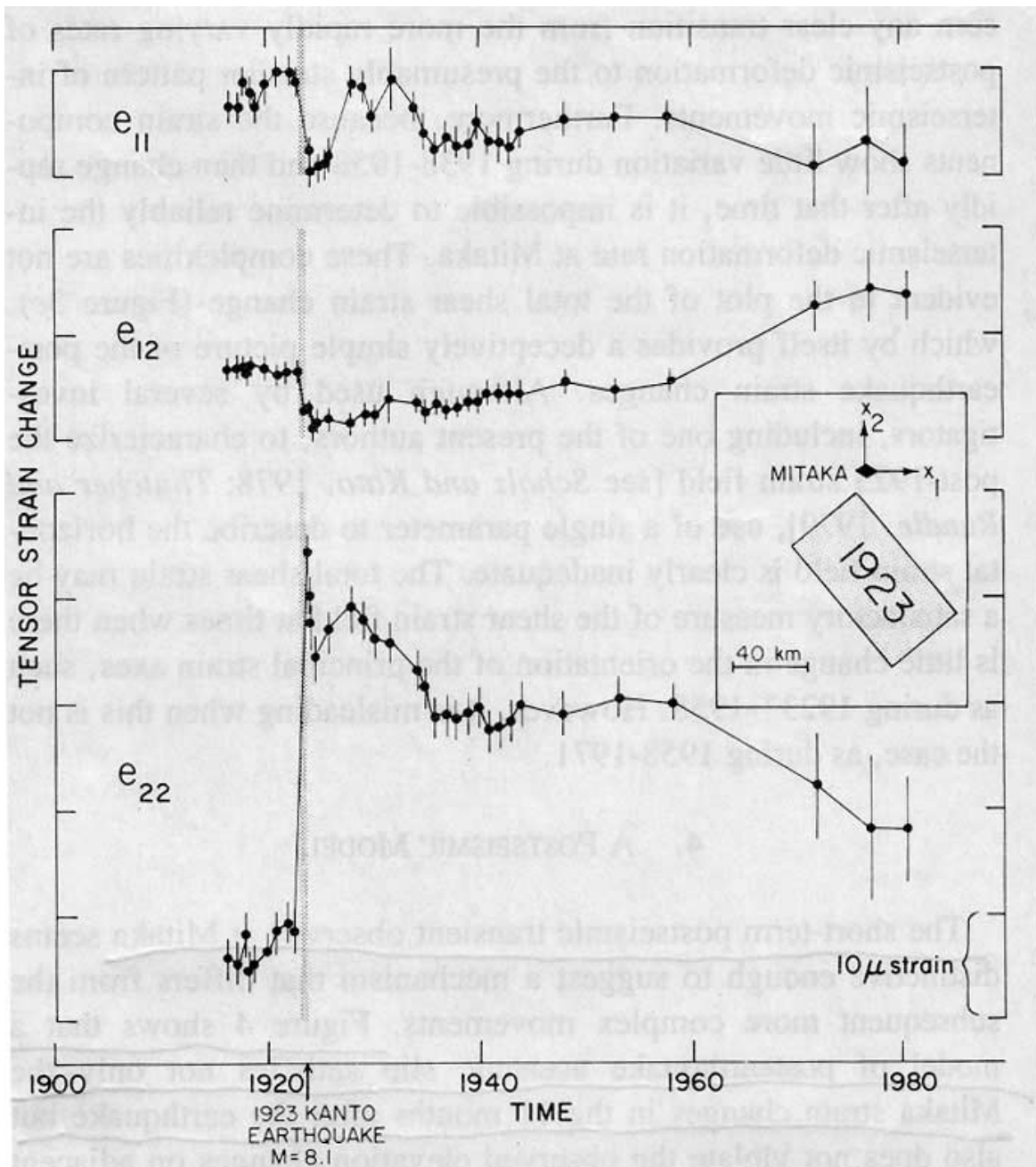


Figure 5



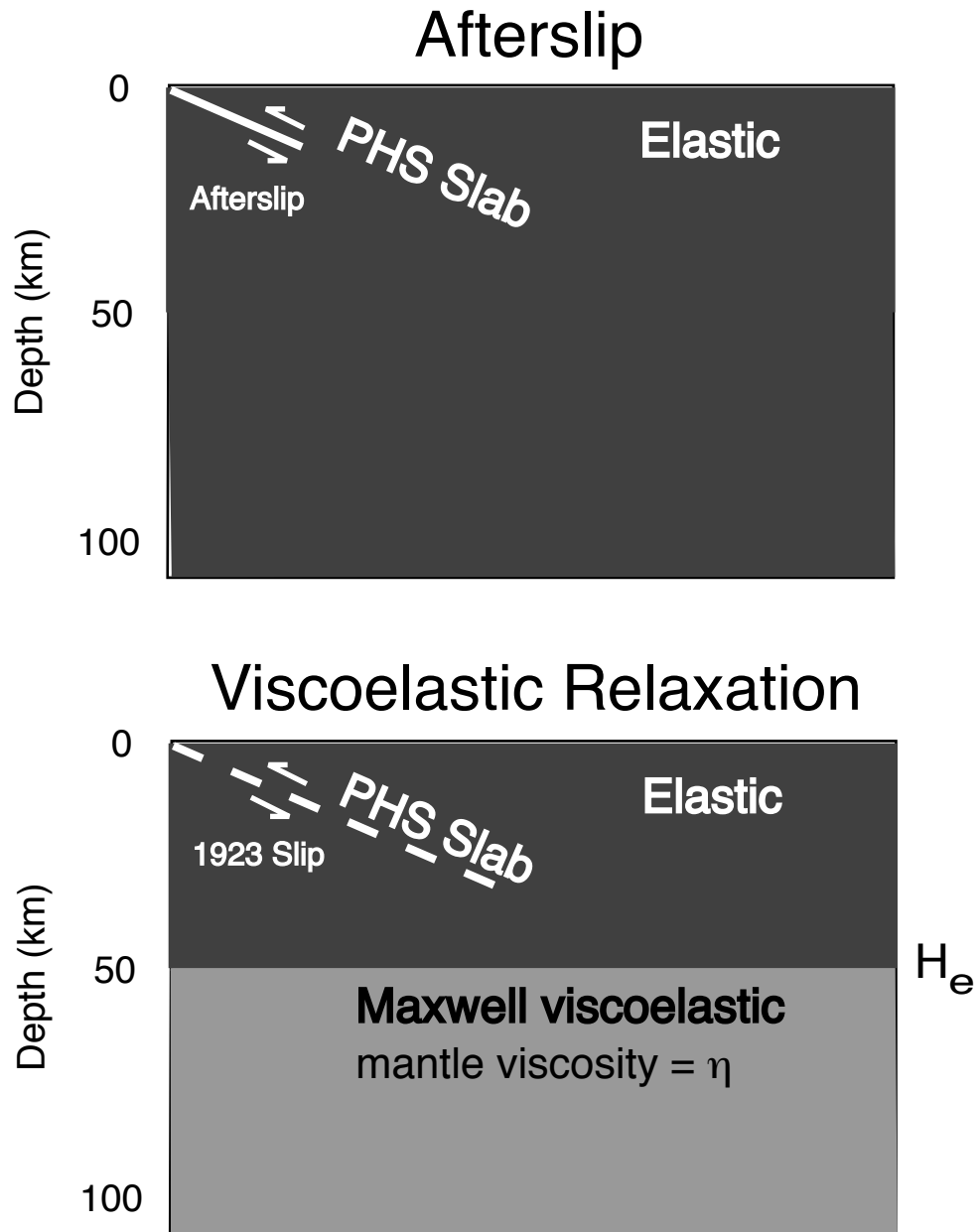


Figure 7

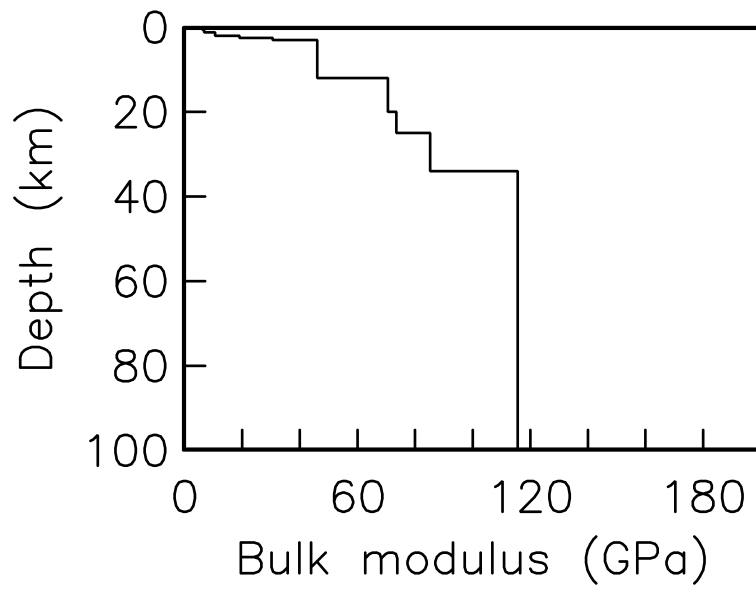
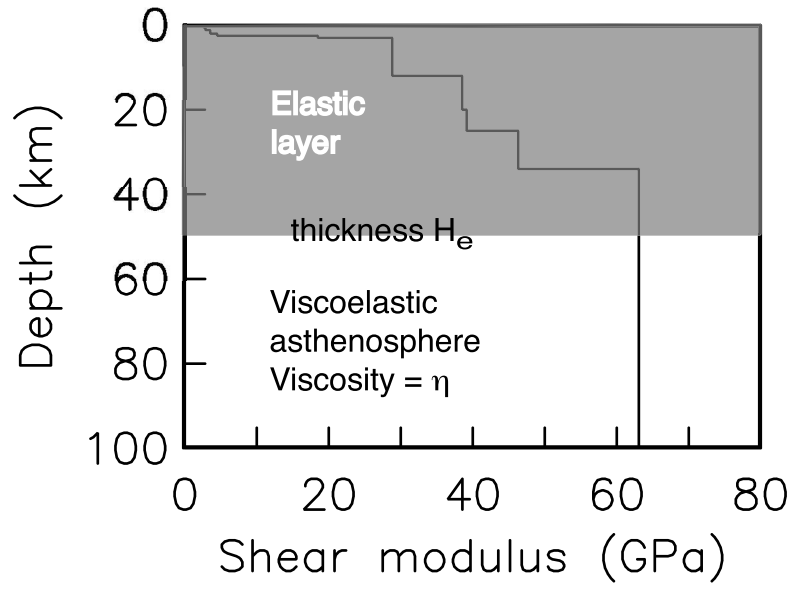
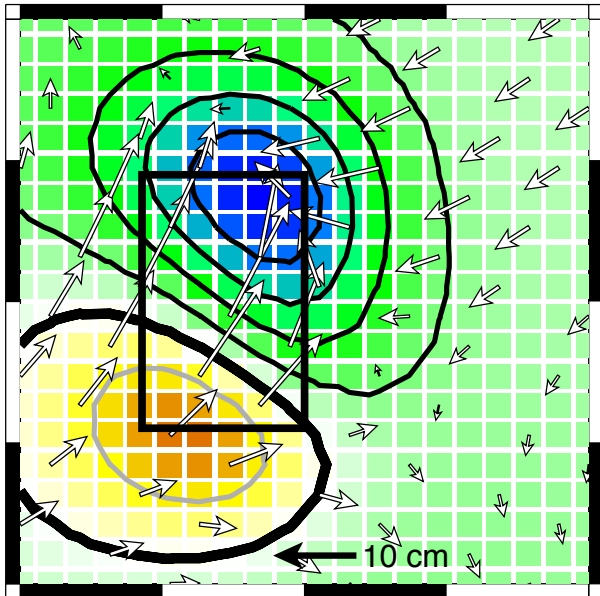


Figure 8

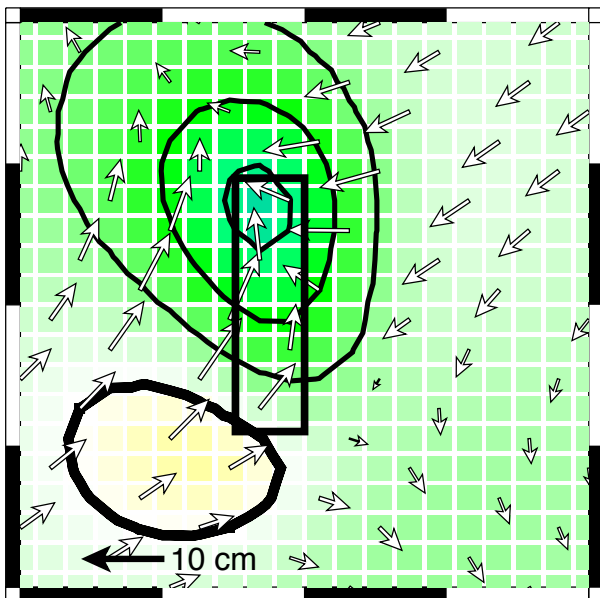
Postseismic Displacement Field

First 7 years (1924-1931)

mantle viscosity= 10^{19} Pa s



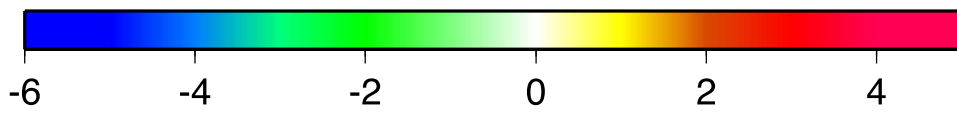
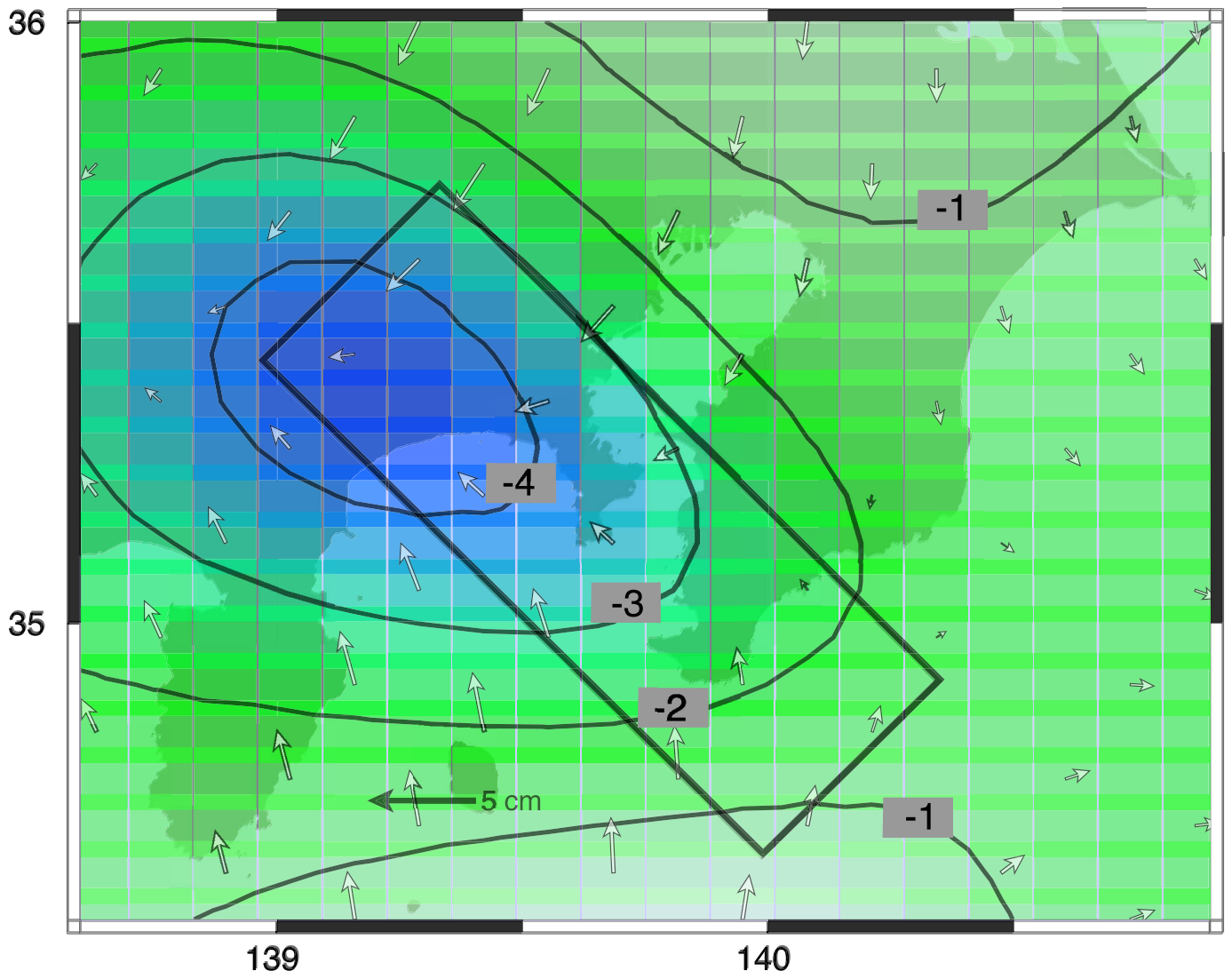
Rake=153 Dip=23
Uniform Slip = 4m from 5 - 30 km
 $H_e = 50$ km



Rake=153 Dip=45
Uniform Slip = 4m from 5 - 30 km
 $H_e = 50$ km



Figure 9



Uplift (cm)

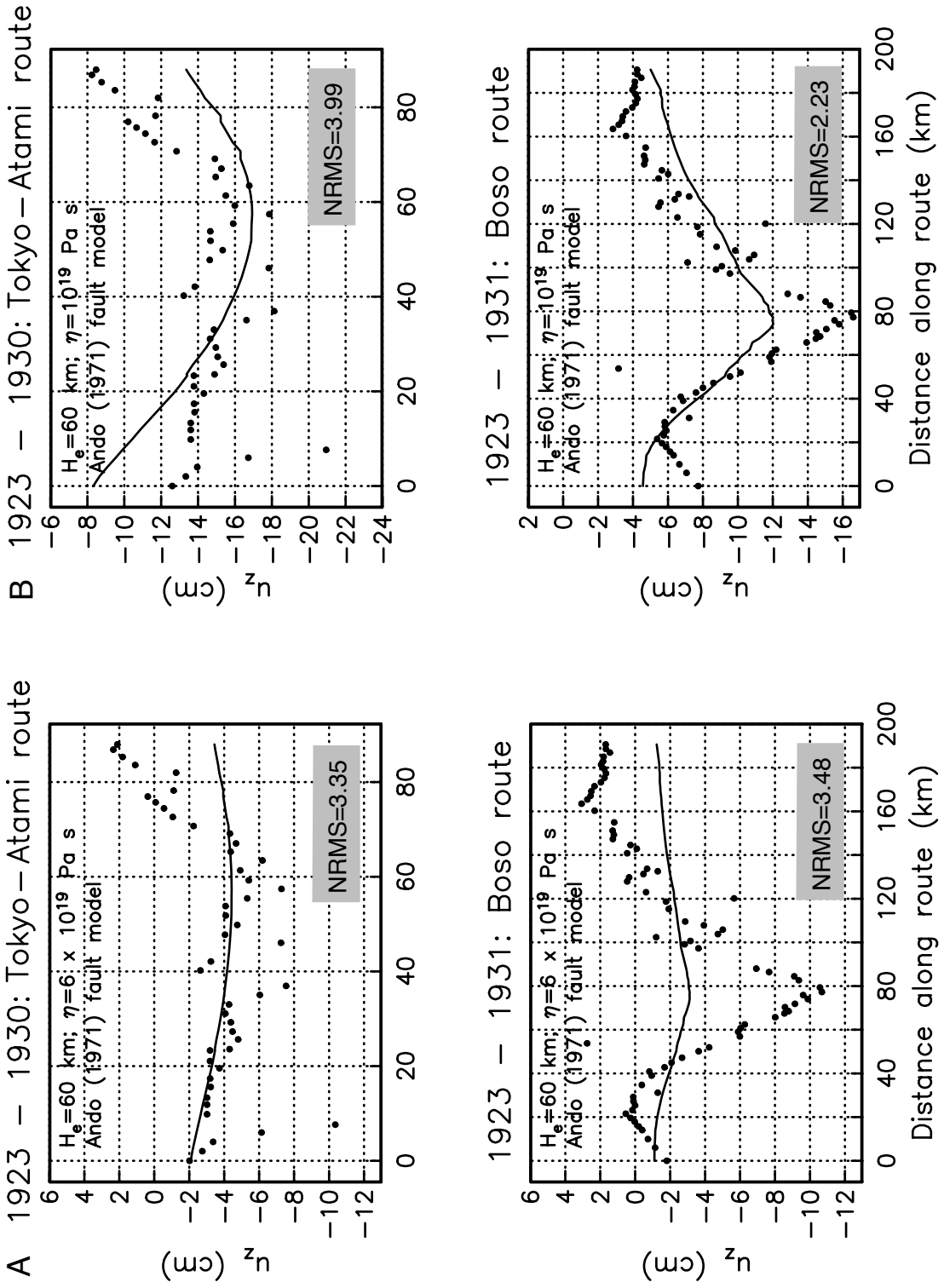
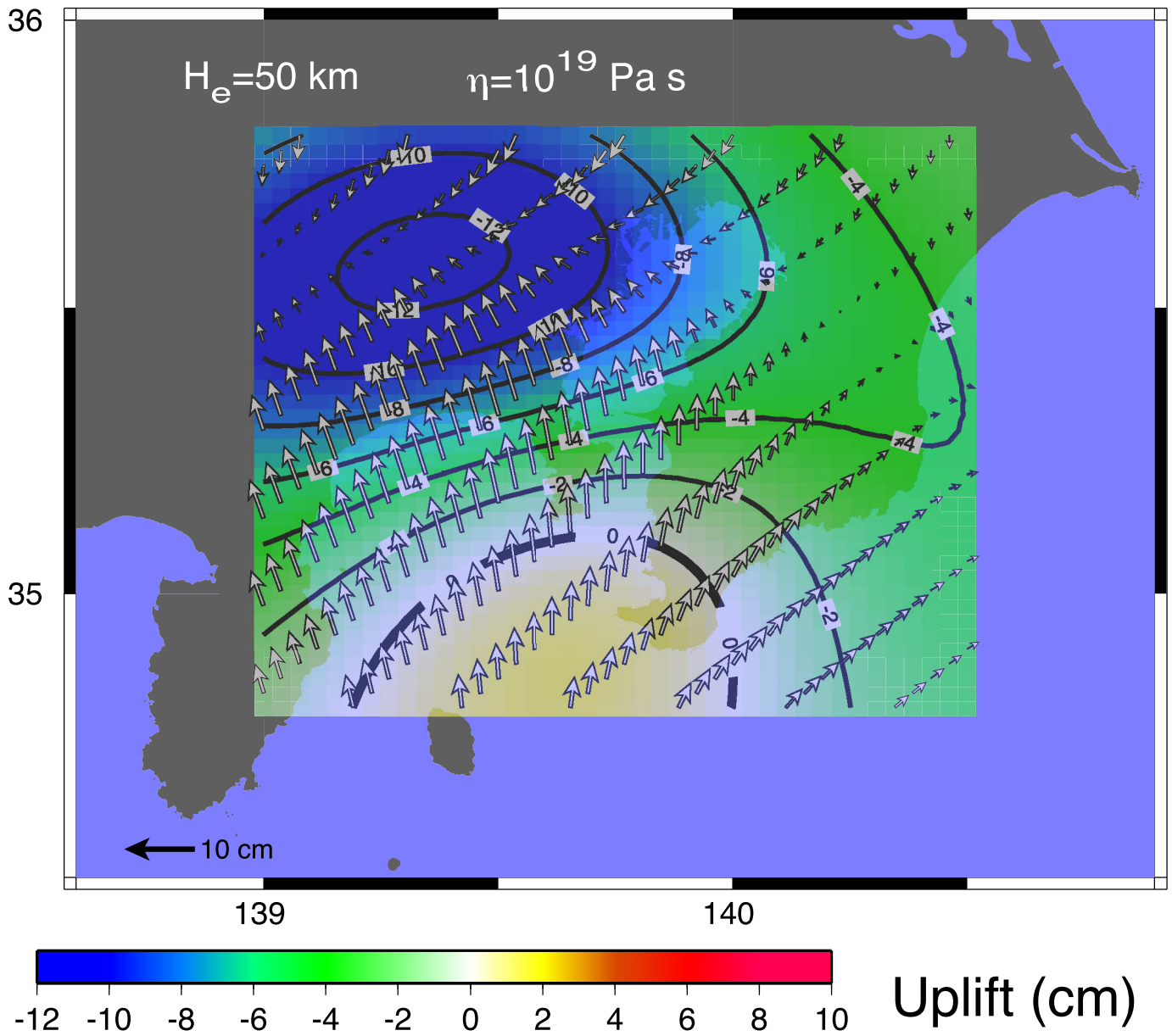


Figure 11



A 1923 – 1931: Boso route

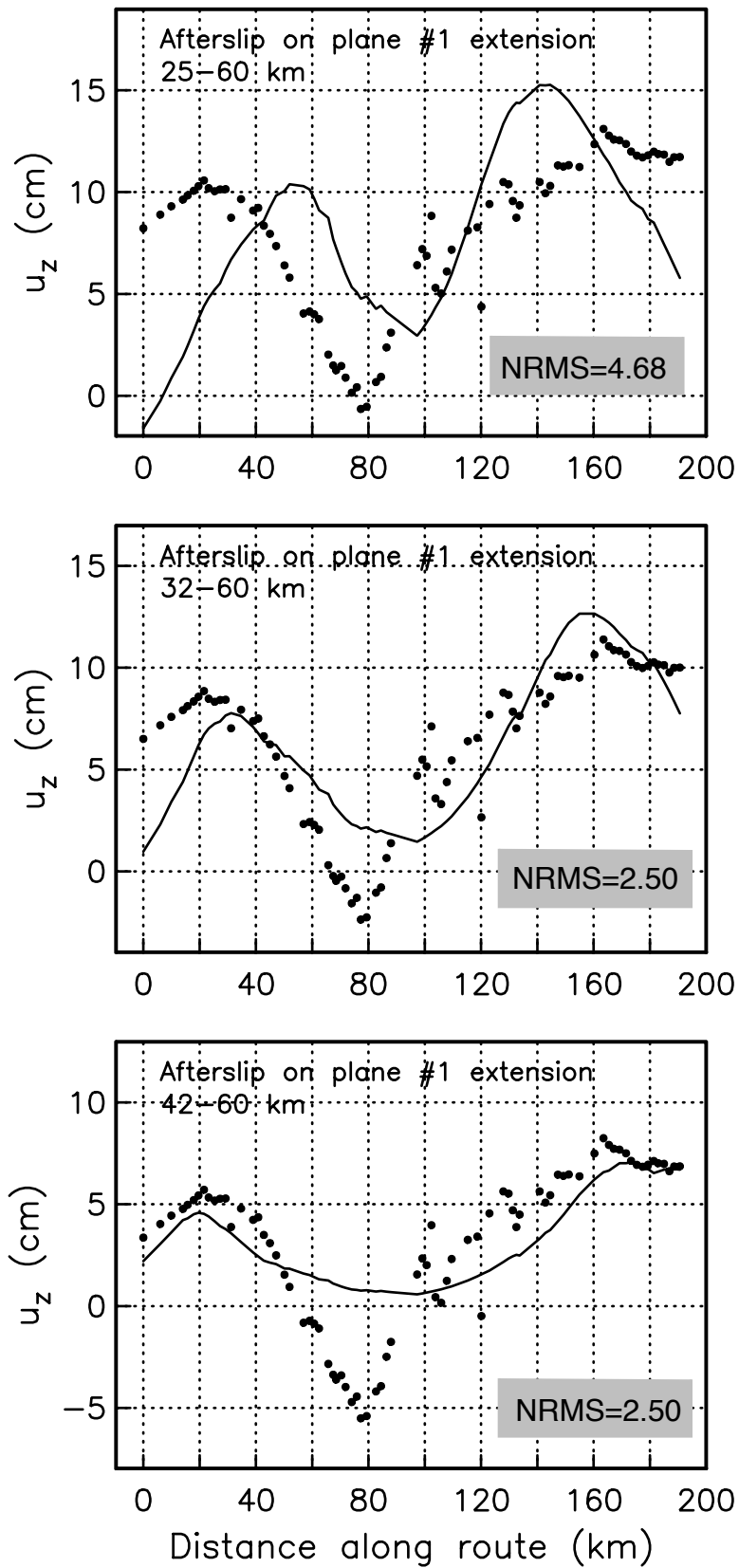


Figure 12

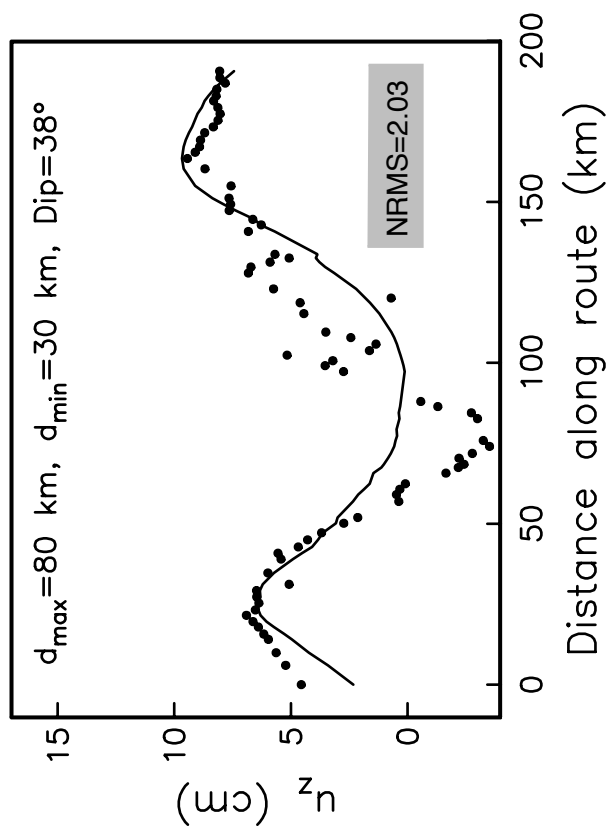
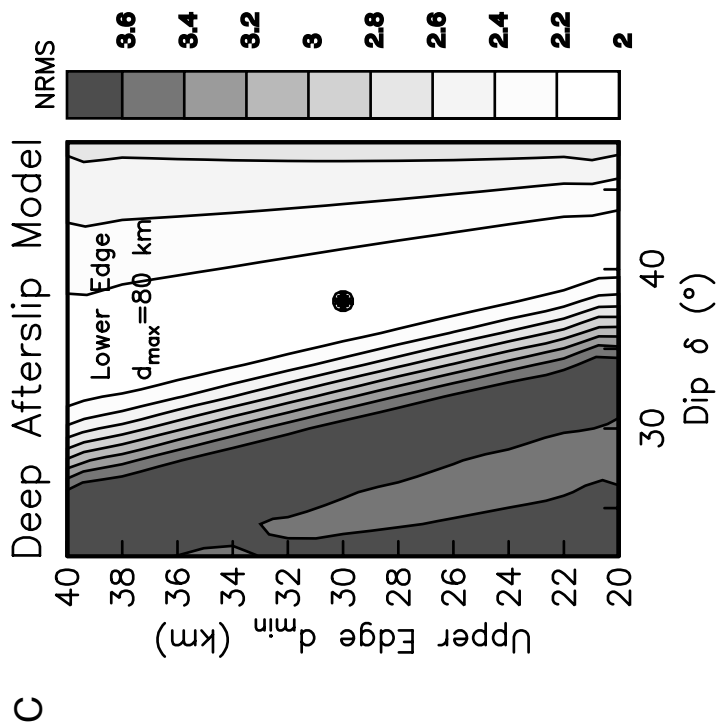
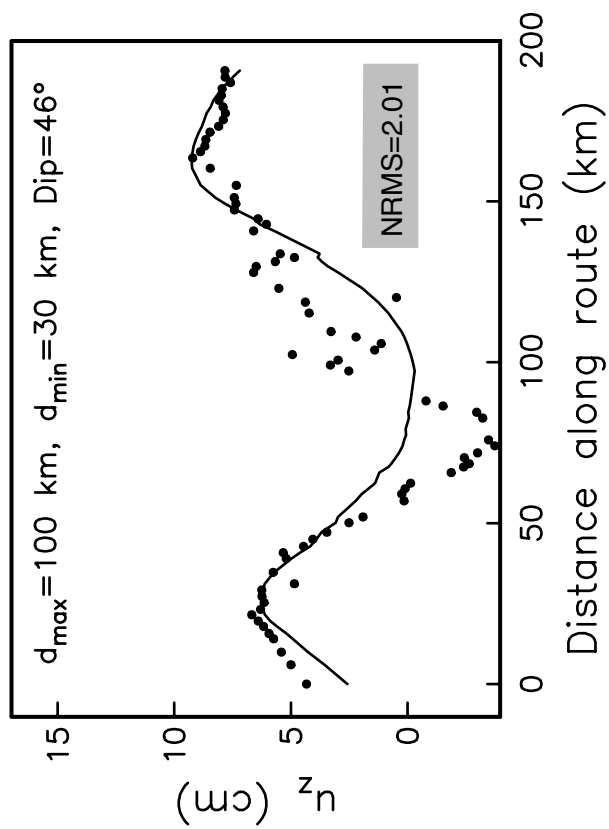
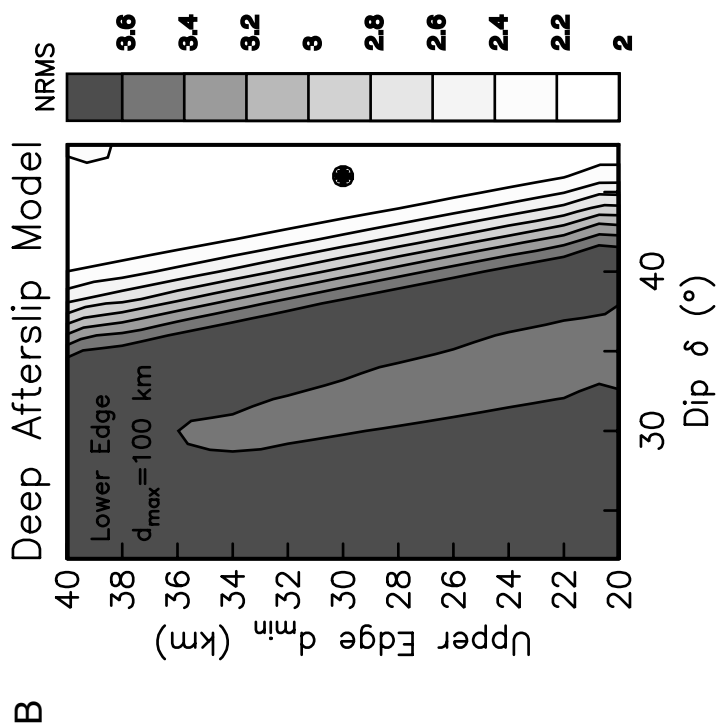


Figure 13

A

B

1923 - 1931: Boso route

1923 - 1930: Tokyo-Atami route

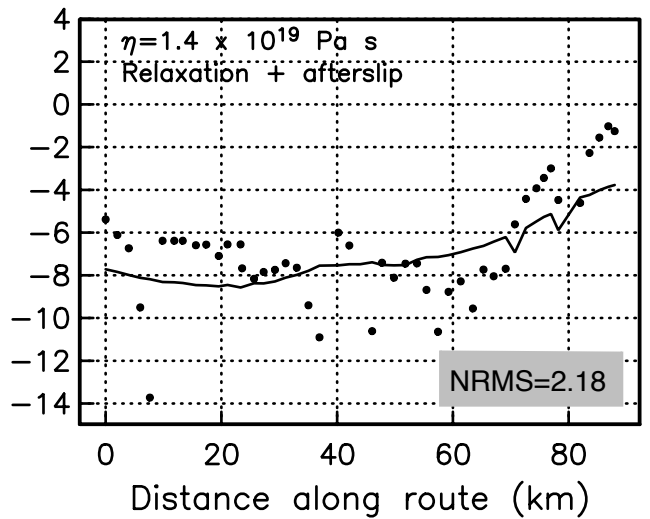
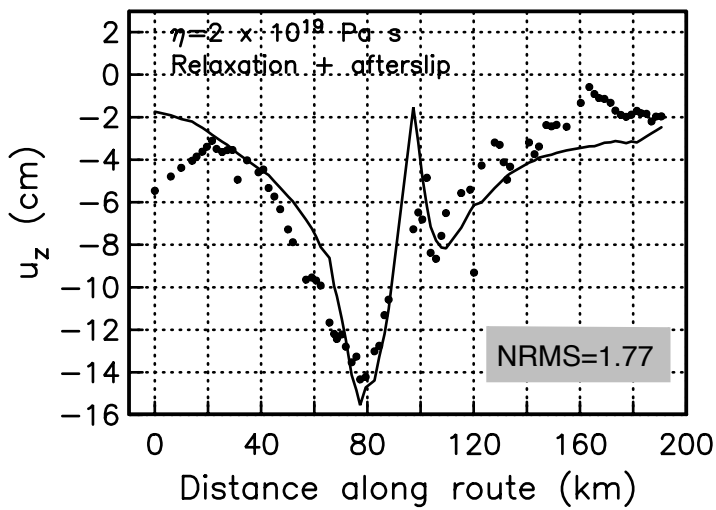
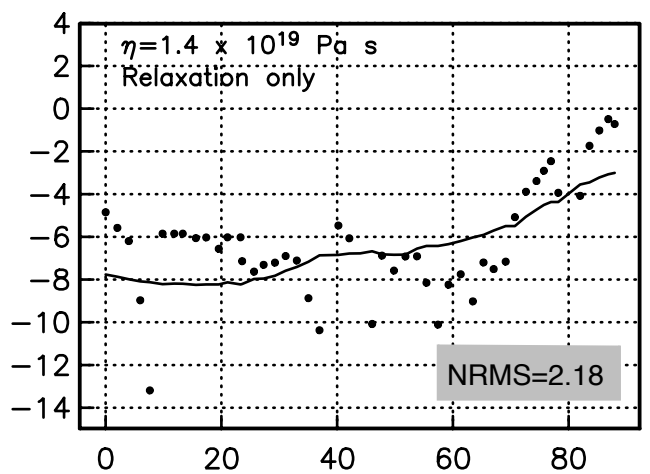
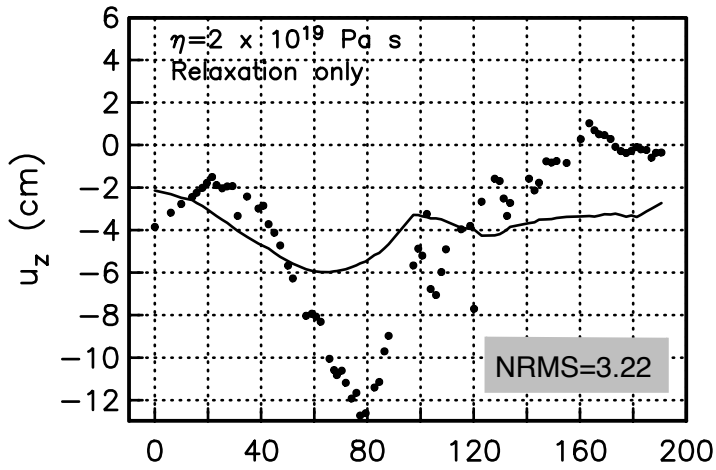
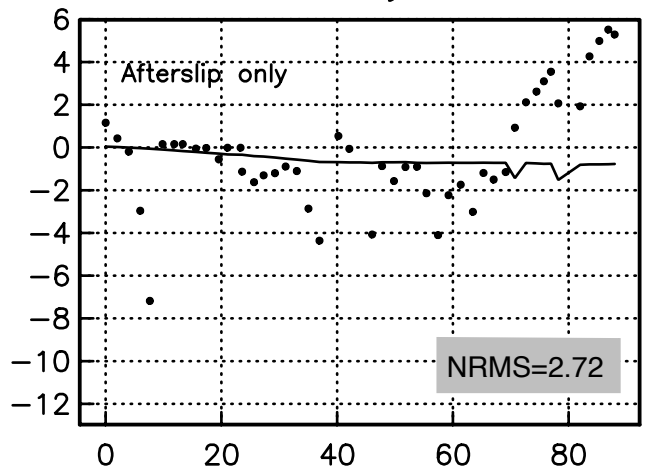
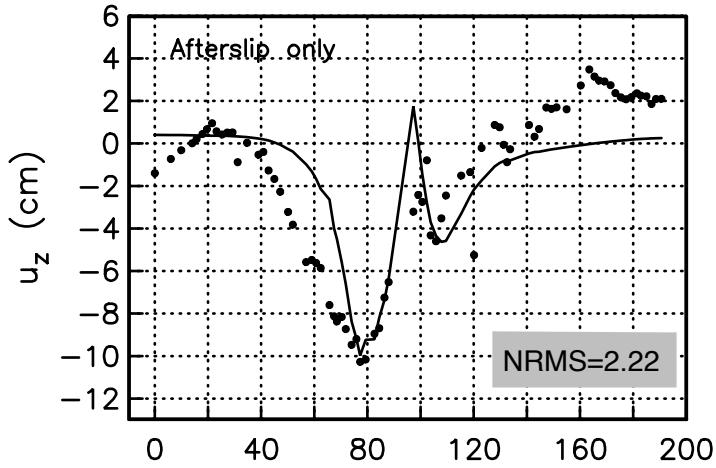
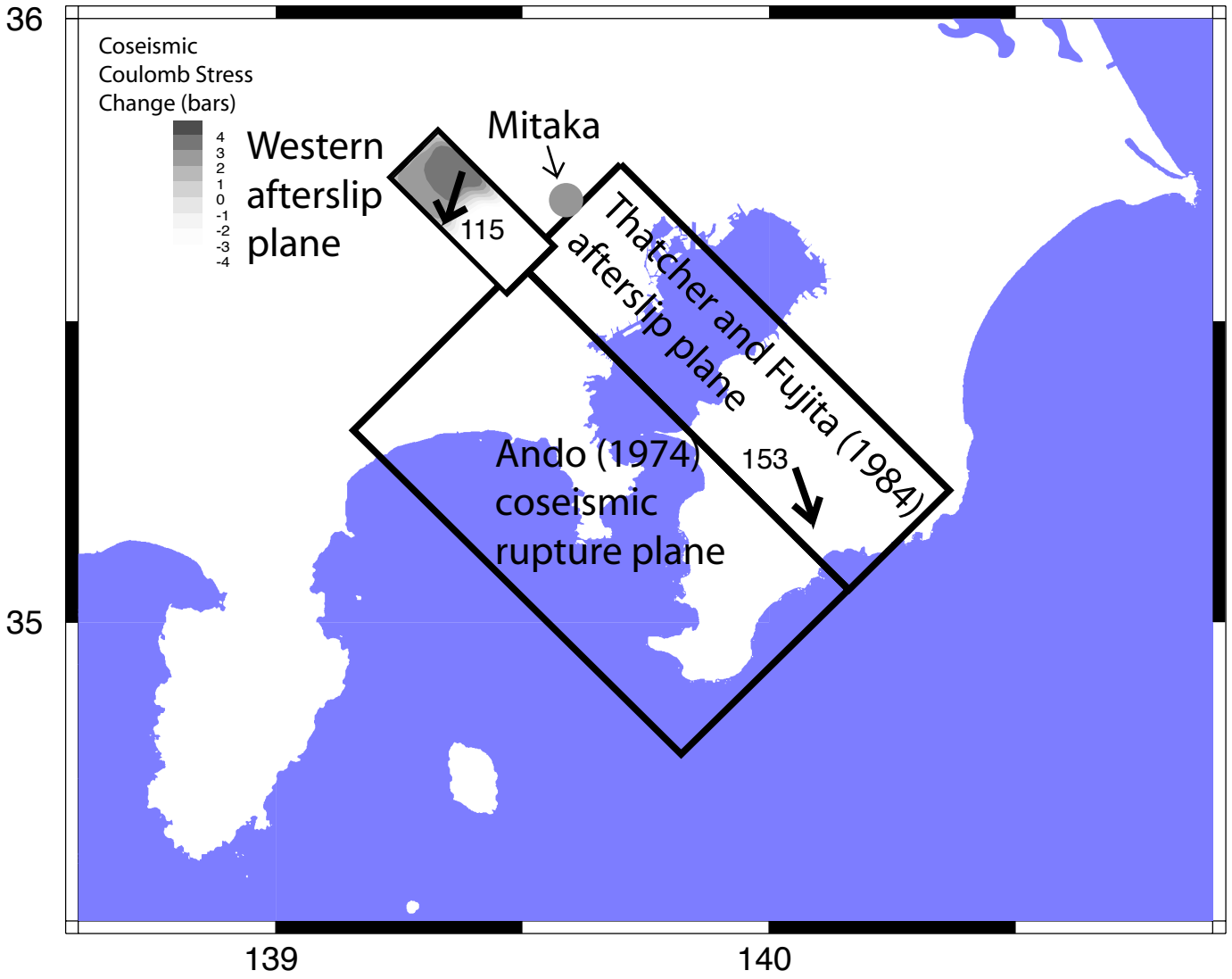


Figure 14



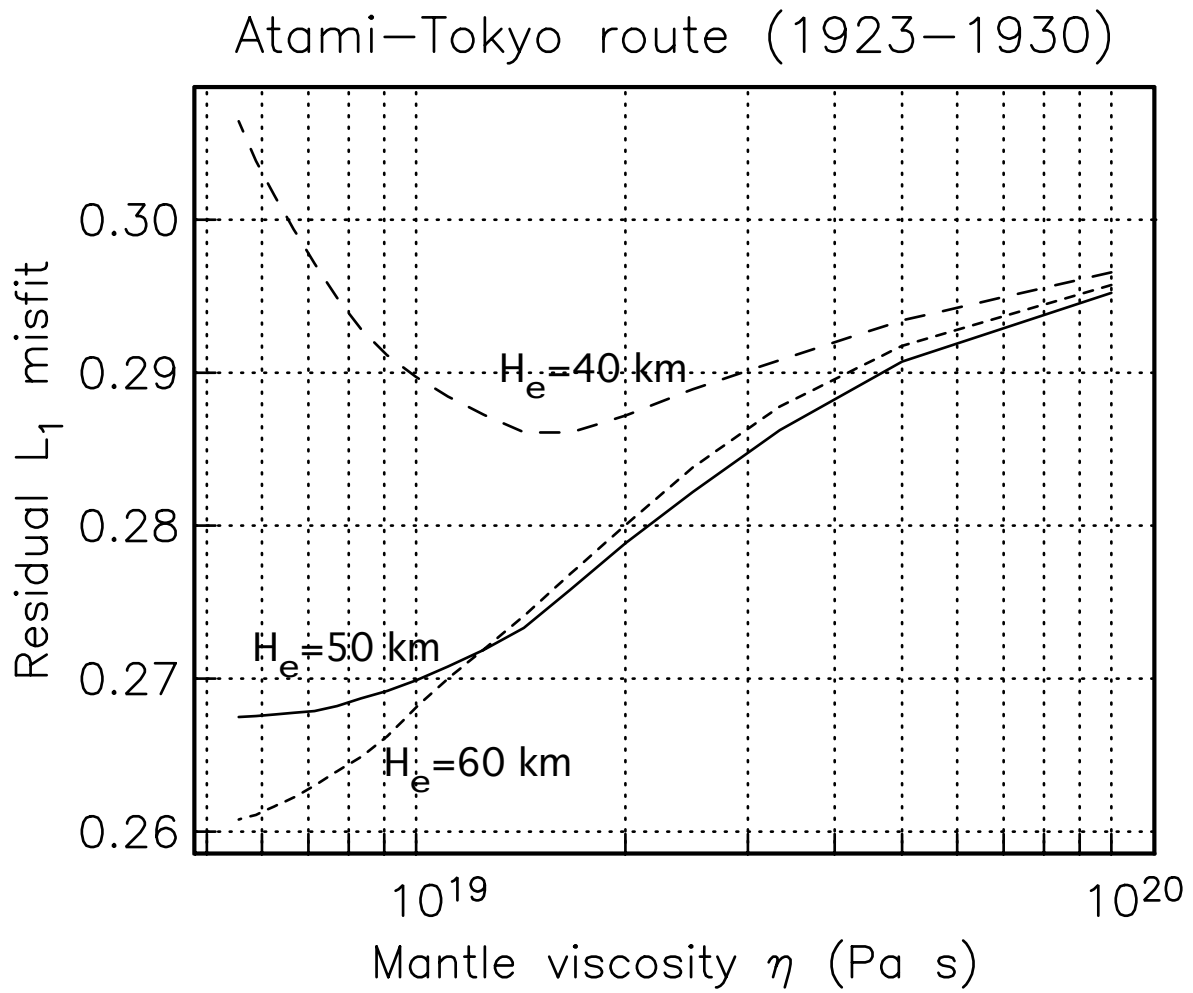


Figure 16

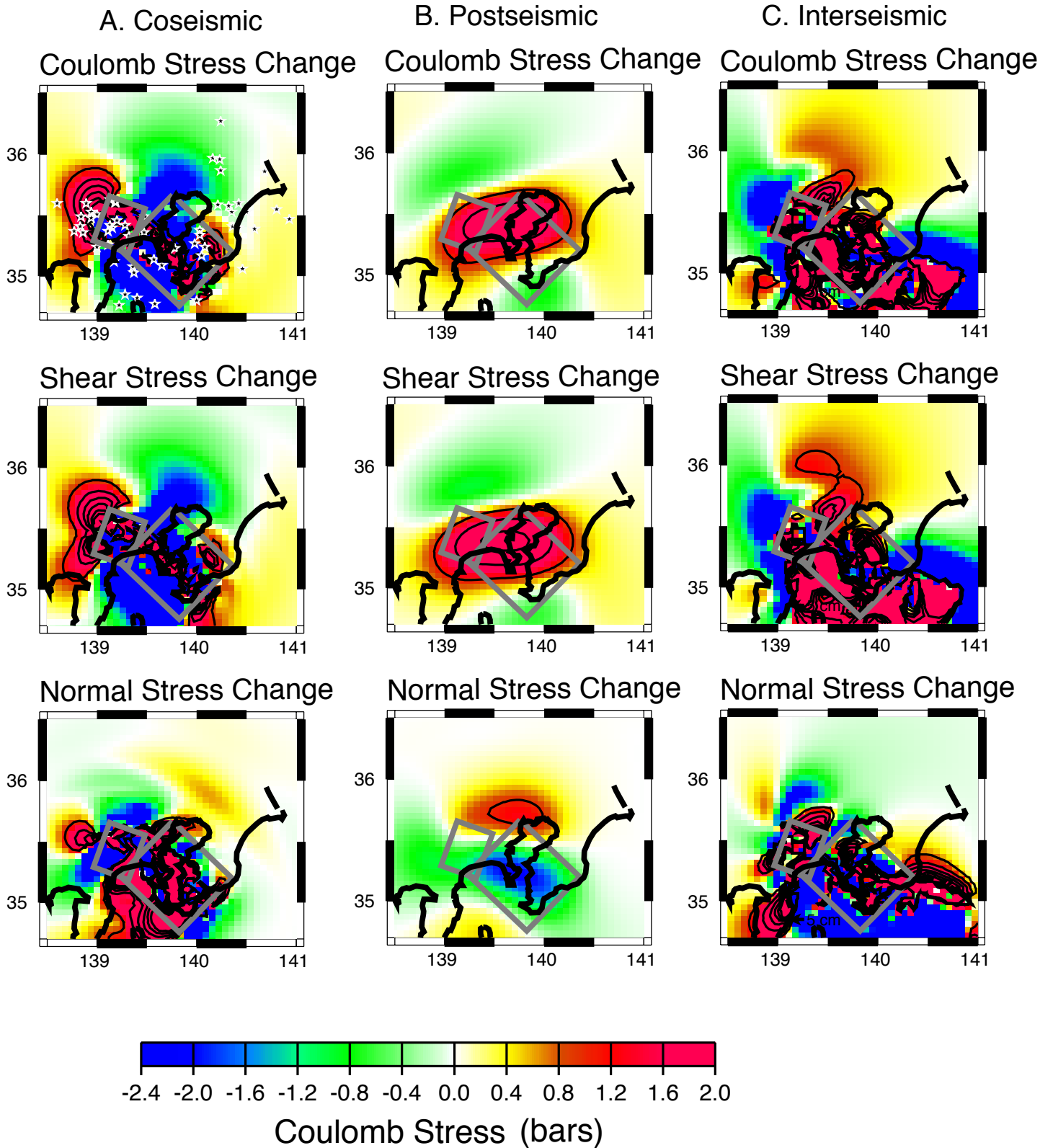


Figure 17

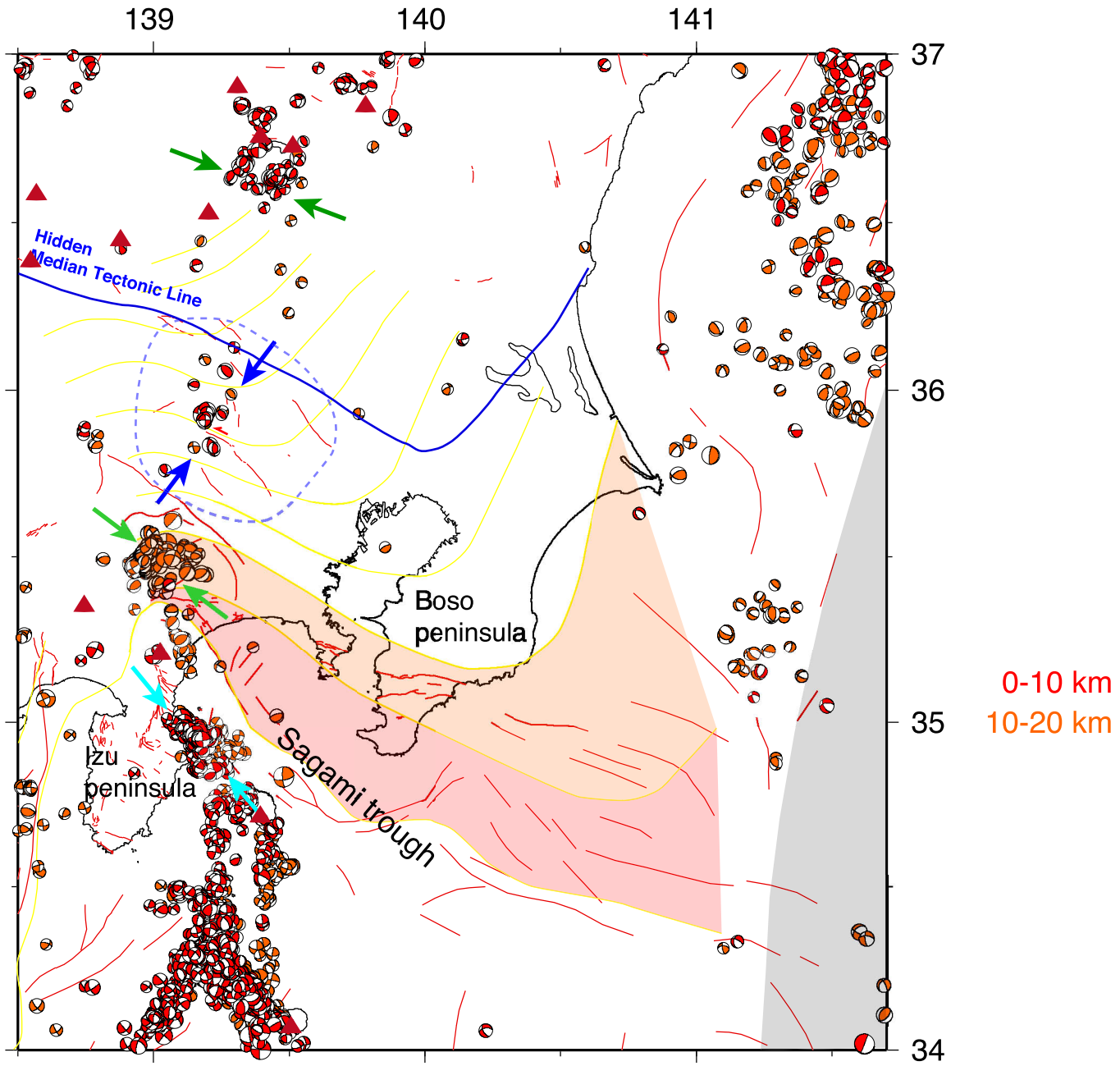
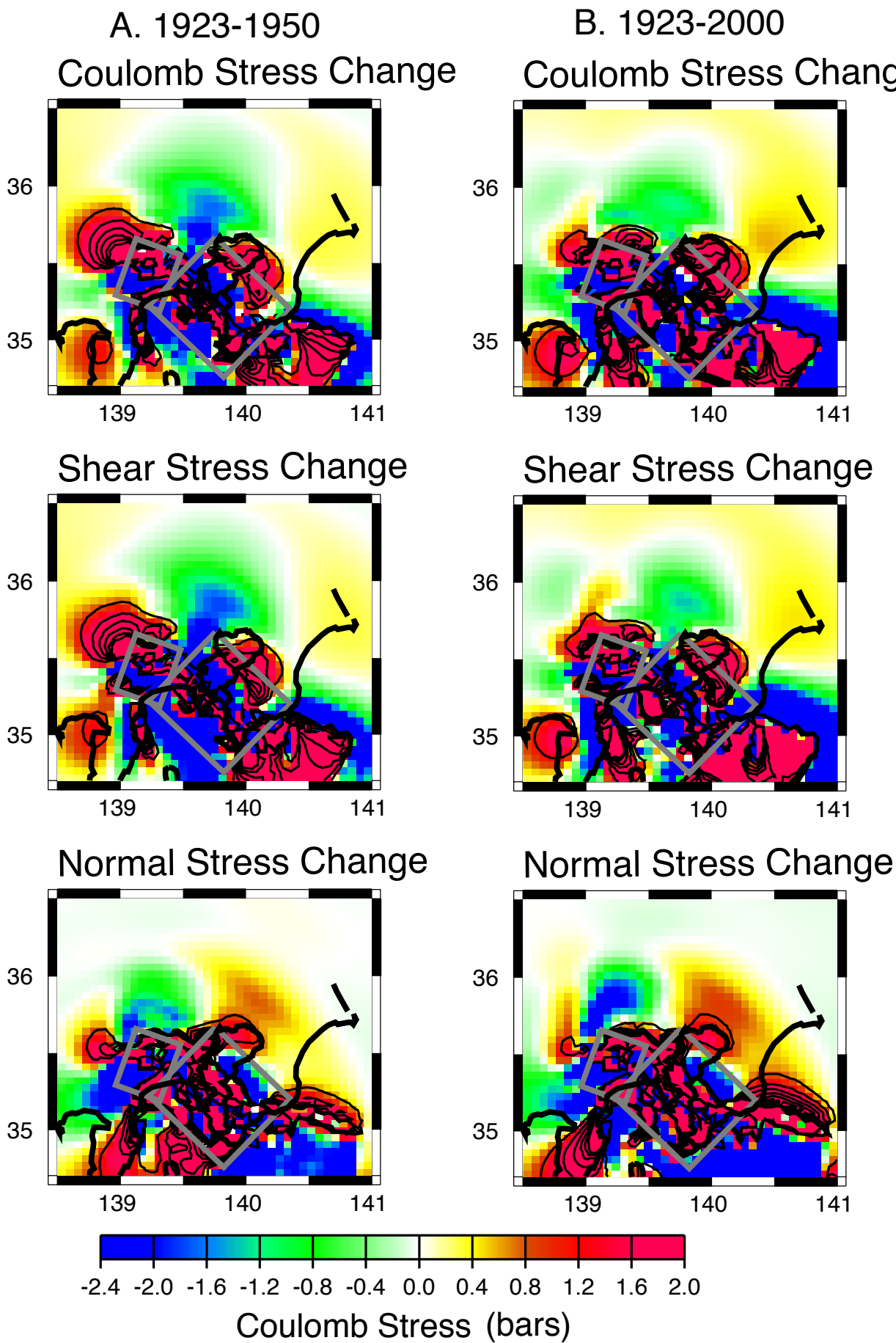
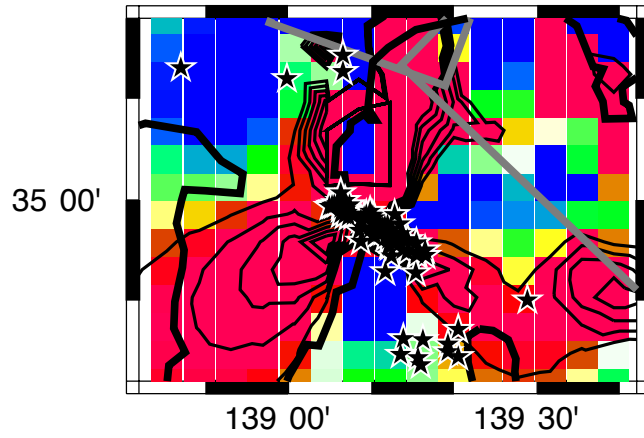


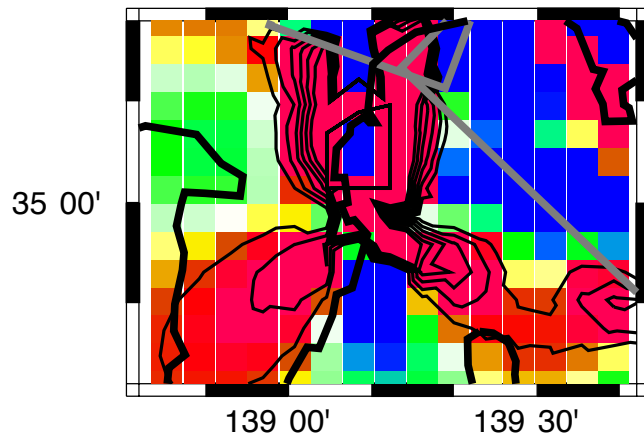
Figure 18



Coulomb Stress Change



Shear Stress Change



Normal Stress Change

